RI.
SE

DIVISION SAFETY AND TRANSPORT

Early Detection of Thermal Runaway in Lithium-Ion Batteries

Ola Willstrand, Oskar Grönlund, Anna Karlsson

RISE Report 2026:114

Early Detection of Thermal Runaway in Lithium-Ion Batteries

Ola Willstrand, Oskar Grönlund, Anna Karlsson

© RISE Research Institutes of Sweden

Abstract

Early Detection of Thermal Runaway in Lithium-Ion Batteries

Thermal runaway (TR) in lithium-ion batteries represents a major safety challenge for electric vehicles, battery energy storage systems, and other electrified applications. This project evaluated technologies and methodologies for providing early warning of battery failure before or during the onset of TR. The work combined a comprehensive literature review with laboratory sensor evaluations, controlled battery cell abuse tests, and full-scale battery electric vehicle (BEV) fire tests. The literature review identified substantial variability in gas generation and failure characteristics as functions of cell chemistry, state of charge (SOC), trigger method, and environmental conditions. Volatile organic compounds (VOCs), electrolyte vapours, hydrogen, and carbon monoxide were identified as key detection targets, while electrochemical impedance spectroscopy (EIS) emerged as a promising technique for detecting internal degradation prior to gas release from the cell. Metrological evaluation of three gas-sensing technologies demonstrated that realistic battery off-gas mixtures strongly influence sensor performance. Furthermore, twenty-two large-format cell abuse tests showed that failure behaviour depends strongly on chemistry, SOC, and heating rate. Electrolyte vapours dominated early venting emissions and sensors designed for electrolyte vapours and VOC detection consistently alarmed earliest. EIS detected internal degradation 15–37 minutes before TR in slow-heating scenarios, outperforming gas-based methods. Full-scale BEV tests confirmed that battery-specific off-gas detectors can provide rapid warning in realistic fire scenarios and that sensor placement significantly affects response time. Overall, the results indicate that robust TR detection requires a multi-layered strategy combining battery diagnostics, sensitive off-gas detection, and conventional fire detection technologies to support effective battery safety management and emergency response efforts.

Keywords: battery safety, early warning, battery failure, fire detection, electrolyte vapours, gas sensors, electrochemical impedance spectroscopy

RISE Research Institutes of Sweden AB

RISE Report 2026:114
ISBN: 978-91-90193-49-5

© RISE Research Institutes of Sweden

Content

Preface **4**
Extended Summary **5**
Literature review 5
Gas sensors evaluation tests 6
Battery cell-level tests 7
Battery electric vehicle tests 9
Conclusions 10
Outlook 11

Appendix 1: Literature review
1 Introduction **1**
2 Gas composition and volume **1**
2.1 Battery vent gas versus combustion gas 2
2.2 Battery vent gas composition 3
2.3 The effect of cell chemistry 5
2.4 The effect of cell format 7
2.5 The effect of cell capacity 7
2.6 The effect of state of charge 8
2.7 The effect of TR trigger method 8
2.8 The effect of cell aging 9
2.9 Conclusions on gas composition and volume 9
3 Gas sensors **10**
3.1 Performance assessments of gas sensors (metrics) 10
3.2 Test methods and test procedures 12
3.3 Relevant applications 14
3.4 Sensor technology – advantages/disadvantages for each sensor type 15
3.5 Conclusions on gas sensors 21
4 Electrochemical impedance spectroscopy **23**
4.1 EIS for early detection of thermal runaway 24
5 Review on thermal runaway detection tests **27**
5.1 Single cell tests 27
5.2 Multiple cells or system level tests 32
5.3 Conclusions on early detection tests 35
6 References **37**

© RISE Research Institutes of Sweden

Appendix 2: Gas sensors evaluation tests

1 Introduction....1
2 Methodology....1
2.1 Sensors....1
2.2 Rig operating conditions/parameters....2
2.3 Experimental Procedure....4
3 Results....8
3.1 MPS sensor evaluation....8
3.2 NPS sensor evaluation....12
3.3 AI prediction sensor evaluation....17
4 Conclusions....18

Appendix 3: Battery electric vehicle tests

1 Introduction....1
2 Methodology....1
2.1 Test setup....2
2.2 Experimental procedure....4
3 Results....4
3.1 General observations....4
3.2 Gas and smoke sensors response....5
4 Conclusions....9

© RISE Research Institutes of Sweden

Preface

This report is a final summary report of the project “Early detection of thermal runaway in lithium-ion batteries (EDOT)”, a partnership between RISE Research Institutes of Sweden and the Electrochemical Safety Research Institute (ESRI) of UL Research Institutes, who supported and funded the work carried out by RISE. The project also acknowledges the support and collaboration with the COFFEE project during the large-scale electric vehicle tests, a project coordinated by RISE and funded by the Swedish Mercantile Marine Foundation and the Swedish Transport Administration.

The following Extended Summary summarises all parts of the project, including:

- **A literature review** (appendix 1)
- **Gas sensors evaluation tests** (appendix 2)
- **Battery cell level tests** (manuscript submitted to scientific journal, reference will be added when published)
- **Battery electric vehicle tests** (appendix 3)

In addition, the Extended Summary ends with overall conclusions from the project and recommendations for future work.

© RISE Research Institutes of Sweden

Extended Summary

Literature review

Thermal runaway (TR) is an uncontrolled increase of battery cell temperature due to exothermic reactions, often triggered by internal short circuits or external abuse. Early indicators may include voltage drop, increased internal resistance, temperature rise, or gas emissions. Depending on the battery failure scenario, early signals for early detection may vary. The literature review presents TR phenomena in lithium-ion batteries (LIBs), with a particular focus on gas generation characteristics and early detection methodologies. It covers experimental data and literature findings across various LIB chemistries, primarily lithium iron phosphate (LFP) and nickel manganese cobalt oxide (NMC) and evaluates the influence of key parameters such as state of charge (SOC), cell format, and thermal abuse conditions, all which influence the possibility of early detection.

Previous literature reviews reveal large variations in the reported gas volumes and compositions during TR events. On average, NMC cells tend to generate larger gas volumes during TR than LFP cells. The gas composition is generally dominated by hydrogen (H_2), carbon monoxide (CO), carbon dioxide (CO_2), volatile organic compounds (VOC) and hydrocarbons (HC), with proportions varying based on TR trigger method, temperature, SOC, cathode composition (notably nickel content) and if the tests were conducted in air or inert atmosphere. Variation in test methodologies, and challenges in distinguishing between vent gases and combustion products, underlines the need for standardized protocols (e.g., UL 9540A) and controlled environments to ensure comparability. However, the varying outcomes of battery abuse tests will also be present in real incidents, which features the importance to fully understand the capabilities and limitations of available detection methods and protocols used.

Each gas sensor technology offers a unique combination of strengths and limitations, making the selection process highly dependent on the specific requirements of the intended application. In the context of early TR detection, choosing the best sensor demands a thorough understanding of the end-user's operational needs. This includes selecting the specific gases to be detected from early stages of TR (e.g., hydrogen, carbon monoxide, hydrocarbons) and determining the optimal sensor location within the system to ensure timely and accurate detection. To ensure that a sensor is fit for purpose, it must be rigorously evaluated against a comprehensive set of metrological performance criteria. These criteria help quantify the sensor's reliability, precision, and robustness under real-world conditions. Key metrics include accuracy, baseline stability, selectivity (or cross-sensitivity), drift, final indication, hysteresis, limit of quantification, linear range, noise, environmental robustness (e.g., temperature, pressure, humidity, dust, vibration), uncertainty, response and recovery time, reversibility, resolution, saturation, and sensitivity.

In addition to gas sensing, electrochemical impedance spectroscopy (EIS) can be used as an efficient tool for early detection of battery failures as it has shown quicker response times compared to only gas sensors and thermocouples. Different segments of

© RISE Research Institutes of Sweden

the EIS spectra, i.e. frequencies and features (the real part, imaginary part, absolute value, and phase angle of the impedance), are dependent on different parameters such as SOC, State-of-Health (SOH) and temperature. In the case of early detection of TR, it is thus important to identify what features and frequency ranges that have a strong dependency on temperature, while having no or low dependency on SOC and SOH. Many studies indicate that the phase angle in the mid-frequency range (1 Hz-1 kHz) show most potential for temperature prognostics and thus early detection of TR.

The literature review also provides a summary of previous experimental studies on early detection principles of TR (e.g., VOC, CO_2, H_2, thermal imaging, LIDAR, EIS) across both single-cell and system-level configurations. The findings point out that sensor placement, detection environment, and trigger method are key parameters influencing the time to detection. Gas detection in small and confined spaces, such as inside a battery pack or module, is relatively manageable. Detection in the open or in a large space is a greater challenge. VOC sensors consistently demonstrate the shortest time to detection among gas sensors in slow failure scenarios (with first venting occurring minutes before TR). Faster failure scenarios (TR within seconds after trigger) can be detected relatively fast by most of the gas sensors involved in the reviewed studies. Although rapid EIS was only evaluated in one of the reviewed studies, the results were promising, showing shorter or similar time to detection as VOC-sensors.

Gas sensors evaluation tests

These tests focused on the metrological evaluation of three sensor technologies intended for early detection of TR events. The three sensor technologies assessed were: a Molecular Property Spectrometer (MPS) sensor for flammable gas detection, a Nanoplasmonic Sensor (NPS) for hydrogen detection, and an AI-based prediction sensor designed to identify characteristic gas signatures using machine-learning algorithms.

Experiments were conducted using a dedicated gas-sensor test rig. Two representative gas mixtures, corresponding to low state-of-charge (LSOC) and high state-of-charge (HSOC) battery conditions, were generated and diluted while maintaining LSOC and HSOC characteristic ratios of H_2, CO_2, CO, and CH_4. Gas compositions were verified with gas chromatography coupled to a thermal conductivity detector (GC-TCD), ensuring traceable and accurate reference measurements. Sensor performance was evaluated primarily through trueness (bias) and dynamic characteristics such as response time (T90) and recovery time (T10).

The MPS sensor demonstrated rapid response characteristics, with T90 values between approximately 8–16 seconds and recovery times of 2–8 seconds. However, its quantitative accuracy was strongly influenced by gas composition. Under LSOC conditions, the sensor consistently overestimated the percentage level relative to lower explosive limit (%LEL), exhibiting relative biases of approximately 200%. The results indicated that CO_2 interfered with sensor readings and was apparently interpreted as a flammable component. In contrast, under HSOC conditions the sensor underestimated %LEL, showing relative biases around −50%, likely because CO was not effectively detected. Despite these limitations, the MPS sensor generally exhibited stable operation and fast detection capabilities.

© RISE Research Institutes of Sweden

The NPS hydrogen sensor showed good performance when exposed to pure hydrogen-air mixtures, with measured concentrations closely matching theoretical values. Nevertheless, substantial interference effects were observed when the sensor was exposed to realistic TR gas mixtures. In both LSOC and HSOC tests, hydrogen concentrations were significantly underestimated, with relative biases reaching approximately −88% in LSOC and −73% in HSOC gas mixtures. The presence of CO and CO_2 appeared to suppress the hydrogen response. Dynamic performance also deteriorated in mixed-gas environments, with response times increasing from roughly 10–14 seconds in pure hydrogen to over 150 seconds in some gas-mixture tests. Furthermore, signal instability and drift were observed. Although the sensor generally recovered after exposure to interfering gases, the results demonstrate that cross-sensitivity remains a significant challenge for this technology.

The AI-based prediction sensor provided a different type of functionality. Rather than delivering quantitative gas concentrations, it produced qualitative outputs indicating whether target gases were detected. After training with both LSOC and HSOC gas mixtures, the sensor successfully detected all tested mixtures across the full concentration range. However, because the output was binary (detected/not detected), conventional metrological parameters such as bias, T90, and T10 could not be determined. Consequently, while the technology shows promise for early warning applications, additional data acquisition and evaluation framework is required before its performance can be rigorously quantified.

Overall, the study demonstrates that realistic TR gas mixtures strongly influence sensor performance. Both MPS and NPS technologies suffered from significant cross-sensitivity effects, leading to substantial measurement errors. The AI-based sensor showed qualitative detection capability but lacked quantitative performance metrics. The results highlight the importance of evaluating candidate sensors under representative battery-failure gas compositions and emphasize that interference effects must be carefully addressed before deployment in battery safety systems.

Battery cell-level tests

These tests investigate gas-based sensing technologies and electrochemical impedance spectroscopy (EIS) under controlled single-cell failure scenarios. A total of 22 experiments were conducted using large-format NMC and LFP cells at different SOC and under both fast and slow thermal abuse conditions. The objective was to identify which detection technologies provide the earliest and most reliable warning signals under realistic system-level conditions.

The experiments were performed in a representative battery module mock-up installed within a semi-open enclosure. Two cell chemistries were studied: a 160 Ah NMC811 cell and a 310 Ah LFP cell. Cells were tested at 50% and 90% SOC using either rapid local heating through a Thermal Runaway Initiation Methodology (TRIM) device or slower external heating at 5 °C/min. This approach enabled evaluation of both rapidly developing failures, where TR follows venting within seconds, and slower degradation scenarios, where observable warning signals may precede TR by several minutes.

The results revealed substantial differences in failure behaviour between chemistries and test conditions. The tested NMC cells exhibited more repeatable behaviour and

© RISE Research Institutes of Sweden

generally experienced TR more rapidly than the tested LFP cells. Higher SOC, NMC chemistry, and slow-heating conditions all resulted in greater cell mass loss and higher peak temperatures. While first venting occurred at relatively similar temperatures across both cell types (approximately 135–150 °C), the time between first venting and TR varied considerably. In most HSOC and fast-heating scenarios, TR followed venting within only a few seconds. In contrast, slow-heating scenarios often provided warning windows of several minutes, reaching 4–17 minutes depending on chemistry and SOC. These findings highlight the strong influence of failure mode on the feasibility of early detection.

Comprehensive gas analysis demonstrated that gas composition evolves significantly throughout failure progression. During first venting, electrolyte vapours, particularly dimethyl carbonate (DMC) and ethyl methyl carbonate (EMC), dominated the emissions. In the semi-open enclosure, approximately 1.4 m away from the battery cell, concentrations of these compounds exceeded 100 ppm before TR, whereas CO concentrations generally remained below 40 ppm. As TR developed, gas composition shifted. NMC cells produced high concentrations of CO and HC gases, while LFP cells generated relatively larger amounts of CO_2 and H_2. The results therefore indicate that electrolyte vapours are more suitable early warning indicators than conventional fire-related gases such as CO or H_2, which typically become prominent only near or during TR.

A broad range of gas detection technologies was evaluated, including electrolyte-vapour detectors, VOC sensors, H_2 sensors, CO sensors, LEL detectors, and smoke detectors. Sensor location proved to be one of the most influential factors affecting performance. Sensors mounted inside the battery module consistently achieved the shortest response times, often detecting abnormal conditions within seconds after venting. Detection outside the module was strongly affected by gas dilution, buoyancy, transport dynamics, and detector design. Among the gas sensors, technologies specifically designed to detect electrolyte vapours provided the earliest and most reliable warning signals. The “Li-ion Tamer” sensors and VOC-sensitive detectors frequently detected first venting minutes before TR occurred. In contrast, conventional electrochemical H_2 and CO detectors generally responded close to TR onset because their target gases were absent or present only at low concentrations during first venting. LEL detectors performed even less favourably due to their high alarm thresholds. Smoke detectors showed reliable operation but mainly detected already-developed TR events rather than providing advance warning. The study also showed that detector housing and gas diffusion characteristics can significantly influence detection performance, even when the underlying sensing technology is identical.

In parallel with gas detection, the study evaluated EIS as a diagnostic technique for monitoring internal battery changes during thermal abuse. EIS measurements tracked impedance magnitude and phase angle over frequencies between 1 kHz and 10 Hz and a three-stage warning framework was developed. Stage I identifies abnormal temperature rise through impedance reduction and phase shifts; Stage II indicates onset of solid electrolyte interphase (SEI) decomposition; and Stage III corresponds to severe degradation and imminent internal short circuit. The EIS methodology demonstrated particularly strong early-warning capability. In all six slow-heating tests where EIS was applied, Stage I and Stage II alarms occurred at cell temperatures between approximately 70 and 105 °C, significantly below the temperatures associated

© RISE Research Institutes of Sweden

with first venting (130-150 °C). Consequently, EIS provided warning times ranging from 15 to 37 minutes before onset of TR. These results suggest that EIS can identify hazardous internal conditions before any measurable gas release occurs, providing earlier warning than gas-based methods in slowly developing failure scenarios.

Overall, the study demonstrates that no single detection technology is optimal for all TR scenarios. Electrolyte-vapour sensors offer the best gas-based early detection because electrolyte emissions dominate during first venting. However, sensor performance depends strongly on location, alarm thresholds, and environmental dilution effects. EIS provides an even earlier indication in slow-heating scenarios by detecting internal electrochemical degradation before gas release. Combining EIS-based diagnostics with sensitive gas detection technologies could offer a robust and comprehensive strategy for TR detection, enabling both early intervention and improved battery safety system design.

Battery electric vehicle tests

These tests were conducted within the framework of another project (referred to as COFFEE) with support from the EDOT project. The COFFEE project investigates the effectiveness of CO_2 total-flooding systems for suppressing vehicle fires in enclosed cargo spaces on ships, while the objective of the EDOT project in these tests was to evaluate the response time and performance of various gas and smoke detection technologies during battery electric vehicle (BEV) fire incidents.

Two separate tests were conducted using representative passenger BEVs. One vehicle (BEV1) employed LFP pouch cells, while the second (BEV2) used NMC prismatic cells. The vehicles were placed inside a purpose-built enclosure designed to simulate an enclosed vehicle space on a ship. Initially, before activation of the CO_2 suppression system, the compartment ceiling was open. TR was initiated in the batteries either through mechanical nail penetration or, when unsuccessful, by applying an oxy-acetylene cutting torch. The battery state of charge was approximately 90%.

Fires were allowed to develop until reaching approximately 2 MW total heat release rate, at which point the enclosure was sealed and flooded with CO_2. The suppression system consisted of multiple CO_2 cylinders capable of producing approximately 45 vol-% CO_2 in the enclosure, corresponding to an oxygen concentration of about 11.5 vol-%. Testing continued for approximately two hours after suppression, followed by venting and observation for potential reignition.

Within the framework of the EDOT project, four different sensor technologies were assessed: a Li-ion Tamer detector, an electrochemical hydrogen (EC H_2) detector, an electrochemical carbon monoxide (EC CO) detector, and a conventional industrial fire detector incorporating smoke and heat sensing. Sensors were positioned at four locations: near the floor adjacent to the vehicle, inside the vehicle cabin, on a side wall of the test compartment, and in the ceiling of the test compartment above the vehicle.

For BEV1, nail penetration failed to initiate TR, requiring application of a cutting torch. Fire growth was relatively gradual, beginning as localized burning beneath the battery pack before spreading to the vehicle's rear section. BEV2 entered TR immediately after nail penetration and exhibited rapid production of smoke, flames, and burning

© RISE Research Institutes of Sweden

droplets. In both tests, CO_2 flooding successfully extinguished all externally visible flames within seconds, and no reignition was observed during the post-suppression monitoring period.

Sensor performance demonstrated that all evaluated technologies were capable of detecting BEV fire events starting in the battery within a few minutes when located up to 1.5 m from the vehicle. The Li-ion Tamer detector consistently provided the fastest response, alarming within approximately one minute of fire initiation. The EC CO detector generally responded second fastest, while the conventional fire detector and EC H_2 detector showed more variable performance depending on test conditions and sensor location. The slower response of the EC H_2 detector was attributed largely to its higher alarm threshold compared with the EC CO detector.

Sensor placement also influenced detection times. Ceiling-mounted sensors consistently alarmed first, demonstrating that smoke and battery off-gases rapidly migrated upward within the enclosure. Wall-mounted and floor-level sensors also provided early warnings, although with somewhat longer response times. Sensors located inside the vehicle cabin responded substantially later than those positioned outside the vehicle.

Also, usefulness of continuous monitoring after CO_2 discharge was examined. Gas and smoke sensors continued to provide valuable information during suppression; however, the electrochemical CO and H_2 sensors reached their upper measurement limits and therefore could not accurately quantify high concentrations potentially approaching flammability and explosive levels. Sensors with extended measurement ranges are needed to evaluate explosion hazards and post-suppression conditions more effectively.

Conclusions

The project has demonstrated that effective early detection of lithium-ion battery TR may require a combination of technologies and a thorough understanding of battery failure behaviour. The literature review showed that failure characteristics and gas generation during TR varies significantly with battery chemistry, SOC, trigger method, and environmental conditions. This variation explains why not a single sensor is typically enough to reliably detect all failure scenarios.

The metrological evaluation of gas sensors revealed substantial challenges associated with cross-sensitivities and gas-mixture effects. For the tested sensors, while having rapid response, their quantitative accuracy was strongly affected by interfering gases. This might not be vital if only focusing on early warning, but in case the sensors are supposed to give information about the actual levels of flammable gases in a compartment for situational awareness and risk assessment, it is crucial that the concentration measurements are reliable.

Single-cell experiments demonstrated that failure characteristics depends strongly on battery chemistry, SOC, and heating rate. In many cases, high-SOC cells and fast-failure conditions left only a few seconds between first venting and TR. In slower failure scenarios, warning windows of several minutes were observed. Among gas-based technologies, electrolyte-vapour detectors and VOC sensors consistently provided the earliest alarms. Sensor placement was found to be a critical factor, with detectors

© RISE Research Institutes of Sweden

located close to the failing cell significantly outperforming sensors mounted further away. Electrochemical impedance spectroscopy showed particularly strong potential by detecting internal degradation processes before any gas release occurred.

Finally, the vehicle-scale tests confirmed that battery-specific gas detection technologies can provide early warning in realistic BEV fire scenarios. Furthermore, both sensor technology and sensor location significantly influence detection performance.

Outlook

Future research could focus on developing battery integrated or battery external multi-sensor detection systems that combine e.g. EIS measurements, existing battery management system (BMS) data, early warning gas sensing, LEL gas detection, and conventional fire detection technologies. However, for improved data and understanding, additional testing should be conducted under a wider range of realistic failure scenarios, with a wider range of battery cell types and formats, in a wider range of battery system configurations and compartments, as well as evaluating a wider range of different detection technologies. Particular attention could also be paid to understanding how ageing and SOH influence detection signatures and warning times, as well as the influence from compartment size and ventilation.

The metrological performance of gas sensors should be further evaluated using representative battery off-gas mixtures covering a broader range of chemistries and SOC levels. An important question is also how activation of different suppression systems affects the ability to continue detecting and monitoring flammable gases. Challenges relate to direct interference of the suppression agent with the sensors, or through dilution, masking or other modifications of the gas environment affecting detection performance. Improved sensor designs with reduced cross-sensitivity and enhanced environmental robustness are needed.

The promising results obtained with EIS justify further investigation, particularly regarding implementation in commercial BMS. Research should focus on rapid impedance measurement methods, automated alarm algorithms, and validation across large battery populations. An additional aspect of interest is the potential for connectivity between the battery system and the facility's monitoring and control systems.

At the system level, future work should address sensor placement optimisation within e.g. battery packs, electric vehicles, stationary energy storage systems, garages and maritime applications. Finally, additional full-scale tests are good for validation and should then evaluate sensor performance during suppression and post-suppression phases, including measurement of potentially explosive gas concentrations. This would support the development of safer monitoring and emergency response strategies for next-generation battery systems.

© RISE Research Institutes of Sweden

Appendix 1: Literature review

Authors: Oskar Grönlund, Ola Willstrand, Ellen Scott, Karine Arrhenius, Sandra Hultmark, Maximilian Patzauer, Jonna Hynynen

1 Introduction

Thermal runaway (TR) in a battery cell means an uncontrolled increase of cell temperature caused by exothermic reactions inside the cell which causes generation of flammable and toxic gases. Many different causes can lead to TR including external mechanical, electrical or thermal abuse. Internal short circuit can also be a cause and can occur due to either external factors or as a result of manufacturing flaws or aging mechanisms. Depending on the scenario, the early signals and the possibility for early detection will be different. Early signals could be a voltage drop or increased cell resistance, increased cell temperature, or increased cell pressure due to swelling. Depending on the scenario, early signals could also include detection of released gases either by gas pressure build-up outside of the cell or by gas component detection. For a slow temperature increase of the cell, the first venting of the cell can occur minutes before TR, when the pressure relief valve or any weak welding point of the cell opens. However, in many scenarios, e.g. involving an internal short circuit, TR will occur almost instantly after the first venting. For any battery system where confirmation of TR or a battery fire relies on sensors outside of the battery system, single cell TR characteristics are important early signals for evacuation and early intervention. If TR in one cell triggers TR in surrounding cells, referred to as thermal propagation, the scenario may accelerate and cause large fire or explosion within a short timeframe.

2 Gas composition and volume

For early gas detection, the gas temperature and buoyancy, gas composition and gas release rate are important factors. This section will focus on the gas composition and gas volume typically vented in TR scenarios from LFP and NMC batteries, as lithium-ion batteries (LIBs) with these cathode materials dominate the market [1].

In a review by Bugryniec et al. [2], literature data on gas production from various battery chemistries were compiled and analyzed. While the reported values show significant variation, typically 0-1000 L/kWh, the findings indicate that NMC cells generally produce larger gas volume than LFP cells. Table 1 presents the median produced gas volume per kWh at 100% state of charge (SOC) in inert vs air atmosphere.

Table 1. Median values of gas production volumes per kWh of NMC and LFP cells in inert vs air atmosphere [2].

Cell chemistry	Median gas production [L/kWh] Inert atmosphere	Median gas production [L/kWh] Air atmosphere
NMC	570	519
LFP	370	126

© RISE Research Institutes of Sweden

The indicated differences of produced gas volumes [L/kWh] between NMC and LFP cells, and between inert and air atmosphere are uncertain and should be used carefully. It could result from the differences in temperature increase during TR, which is typically lower for LFP cells. However, the compiled data by Bugryniec et al. [2] also showed surprisingly low median gas volumes [L/kWh] produced from NCA cells, (which should be more similar to NMC cells regarding temperature increase during TR). This implies that the differences in the produced gas volume between LFP and NMC can not only be explained by the temperature during TR, but it is also likely to be due to variations in test methodologies. In addition, the number of data points is much larger for NMC cells than for LFP (and NCA) cells. Regarding gas volume differences due to the surrounding atmosphere, it is unclear why the gas volumes are lower in air atmosphere. Again, it may be other factors that are behind those differences. An air atmosphere may contribute to combustion reactions outside of the cell and thereby change the gas composition.

Despite a large number of published studies regarding heat and gas release during TR, relatively few are comparable due to large variations in the test methodology [3]. These variations also make conclusions difficult to establish. Nilsson & Ahlberg Tidblad [4] have listed some important factors which must be considered in future experiments to improve comparability:

1. “Detailed information about the test object, e.g., the cell type and size, cell chemistry, and composition of materials, including electrolyte solvent composition;
2. The TR trigger condition to determine the severity of the abuse;
3. Clarity regarding what gases (e.g., vent gases, combustion gases or a mix) are studied;
4. The timing and method of gas measurement (e.g., direct measurement or delayed measurement on sampled gases) as this affects the chemical history of the gases due to the reactiveness of some species;
5. Controlled gas environment, e.g., turbulent or stationary conditions, inert or air atmosphere, and gas chamber volume;
6. When evaluating the gas measurements, it is also important to consider the possibility of other oxidants in addition to O_2, and it is recommended to perform a mass balance to the greatest extent possible in order to verify the consistency of results.”

2.1 Battery vent gas versus combustion gas

To analyze the gas composition resulting from cell-venting, standardized methods such as UL 9540A [5] can be used. Tests to evaluate the flammable gas composition, in UL 9540A, are performed in an inert environment using nitrogen, N_2. This enables analysis of the non-combusted gases (i.e. battery vent gas). The atmosphere in which the tests are performed will impact the gas composition. Other inert gases such as argon (Ar), helium (He), or mixtures of inert gases have also been reported to be used in experiments [6], [7], [8], [9].

Tests can also be performed in an open test setup (i.e., ambient atmosphere). Here, the gas composition may deviate from the results obtained in the closed/inert test setup since the vented gases may react/combust, resulting in a measurement of combustion

© RISE Research Institutes of Sweden

gases. Typically, an increased fraction of carbon dioxide (CO_2) and a decrease in the fraction of flammable gases are noticed for tests performed in ambient atmospheres [10], [11]. Additionally, in ambient atmosphere and at high temperatures, some tests indicate that chemical reactions with oxygen may significantly increase the fraction of volatile organic compounds (VOCs), along with an increased fraction of carbon monoxide (CO) [12].

2.2 Battery vent gas composition

The main components of battery vent gas during TR are hydrogen (H_2), Carbon monoxide (CO), Carbon dioxide (CO_2), and hydrocarbons (HC) (such as methane, ethane, ethylene etc.) [9], [13], [14]. Hydrocarbons may also be reported as total hydrocarbon content (THC). Figure 1 shows mean concentrations at different SOC for TR in inert atmosphere. One standard deviation is indicated, but the variation is large, and many tests exist with measured concentrations beyond these intervals [13].

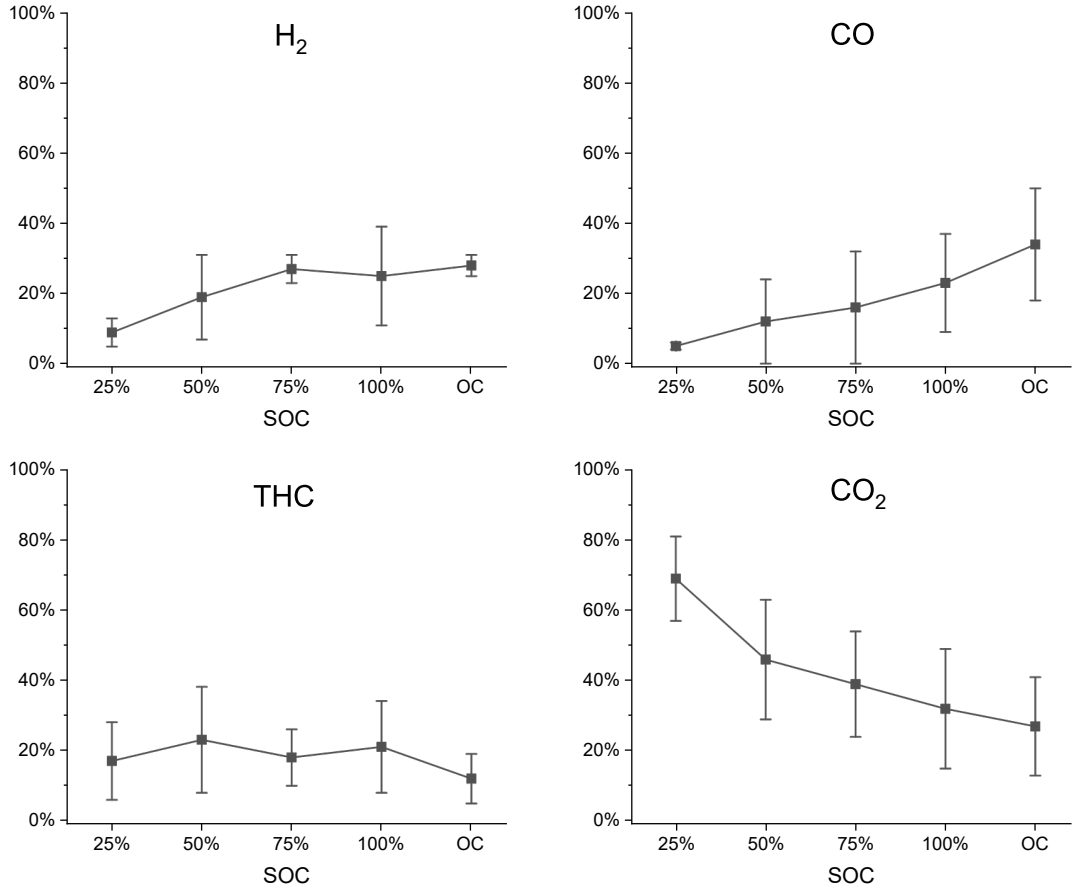

Figure 1. Mean concentrations and one standard deviation of H_2, CO, CO_2 and THC in TR vent gas in inert atmosphere, from literature [13]; OC means overcharge.

Depending on the temperature at venting, the gas composition will vary as depicted in Figure 2 [12]. Note that this figure does not cover all gas generation reaction paths, for example, already at normal cell cycling it is possible to detect H_2, C_2H_4, CO, CO_2 and O_2 inside a cell [15]. This will be a result of side reactions that is part of aging mechanisms in the cell. At temperatures around the boiling point of the electrolyte, and depending on the cell format (e.g., pouch cells lack safety vent), the first stages of cell venting may

© RISE Research Institutes of Sweden

include considerable amounts of electrolyte vapor. At temperatures above approximately 260 °C (500 °F), chemical reactions including multiple battery cell materials will result in more violent reactions and generate considerably larger amounts of gas.

Release of electrolyte vapor is more commonly reported for lithium-iron-phosphate (LFP) than for lithium-nickel-manganese-cobalt oxide (NMC) battery cell types. In work by Yang et al. [16], it was found that the proportion of electrolyte in vent gases was as high as 95% upon nail penetration of cylindrical LFP cells. Note that, despite nail penetration, the maximum cell casing temperatures reached in these tests were between 120 and 160 °C (<320 °F), which explains the high proportion of electrolyte vapor.

Another test performed by Fernandes et al. [17], reached only 150 °C in an overcharged scenario with an LFP cell. As soon as the cell was no longer air-tight, the following compounds were detected in concentrations where DMC > CO2 > EMC > CO > CH4.

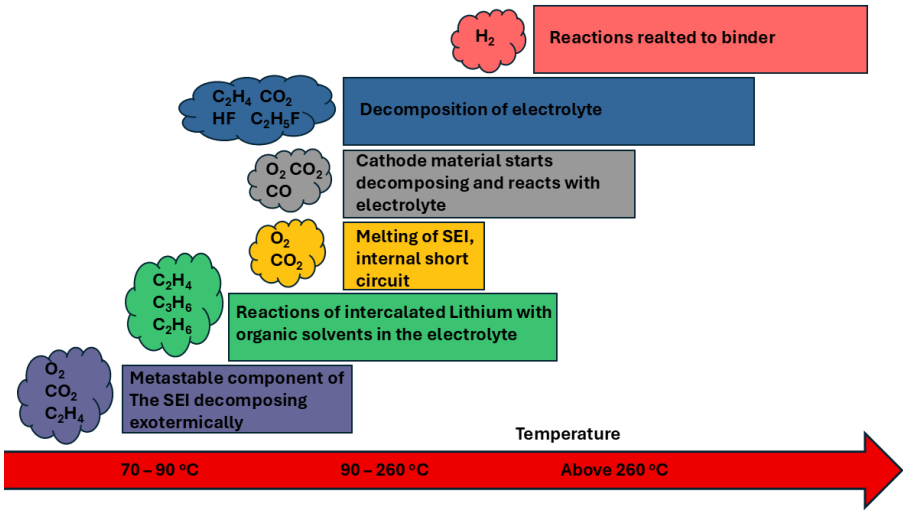

Figure 2. Example of gas emissions at different temperatures. The figure is modified from reference [15].

Organic carbonate solvents are commonly used as electrolytes in lithium-ion batteries. These include for example, ethylene carbonate (EC), dimethyl carbonate (DMC), diethyl carbonate (DEC), propylene carbonate (PC) and ethyl methyl carbonate (EMC). Most of these solvents, except EC and PC, have a boiling point below 130 °C (266 °F). For chemical specifications of different electrolytes see Table 2.

© RISE Research Institutes of Sweden

Table 2. Physical properties of common electrolytes in ambient conditions [18]

Electrolyte	Molecular weight (g mol^{-1})	Flash point (°C/°F)	Boiling point (°C/°F)	Autoignition temperature (°C/°F)	Flammability limits (lower/ upper) (%)
Ethylene carbonate (EC)	88	143 / 289.4	248 / 478.4	465 / 869	3.6 / 16.1
Dimethyl carbonate (DMC)	90	16 / 60.8	91 / 195.8	458 / 856.4	4.2 / 12.9
Diethyl carbonate (DEC)	118	25 / 77	126 / 258.8	445 / 833	1.4 / 11.0
Propylene carbonate (PC)	102	132 / 269.6	242 / 467.6	455 / 851	1.8 / 14.3
Ethyl methyl carbonate (EMC)	104	24 / 75.2	110 / 230	440 / 824	N/A

2.3 The effect of cell chemistry

As already mentioned, the cell chemistry will affect the cell temperature development and thereby the gas composition for different scenarios. Further, there are variations in the gases left after TR depending on the cell chemistry. Figure 3 is based on the same literature data as Figure 1, but only showing mean concentrations for tests with LFP and NCA cells, which shows the largest differences. Note that the data for the NMC cells which contain a similar nickel content as NCA cells also show a similar gas composition, while NMC cells with lower nickel content typically have a lower CO/CO2 ratio [13].

For tests in inert atmosphere, batteries with the same type of cathode material exhibit comparable normalized gas production [12], [13]. However, for NMC, the nickel content for the cathode material may vary. An increased nickel content increases the energy density, which typically also results in a higher gas production volume [19]. Additionally, the TR onset temperature decreases with increasing nickel content. For example, in tests conducted by Shen et al. [19], NMC 9/0.5/0.5 (mutual ratio of Ni, Mn, Co) has a thermal onset temperature of ~ 130 °C, whilst NMC811 ~ 135 °C and NMC523 ~ 143 °C. For LFP the TR onset temperature is often higher than for NMC, ~ 184 °C.

© RISE Research Institutes of Sweden

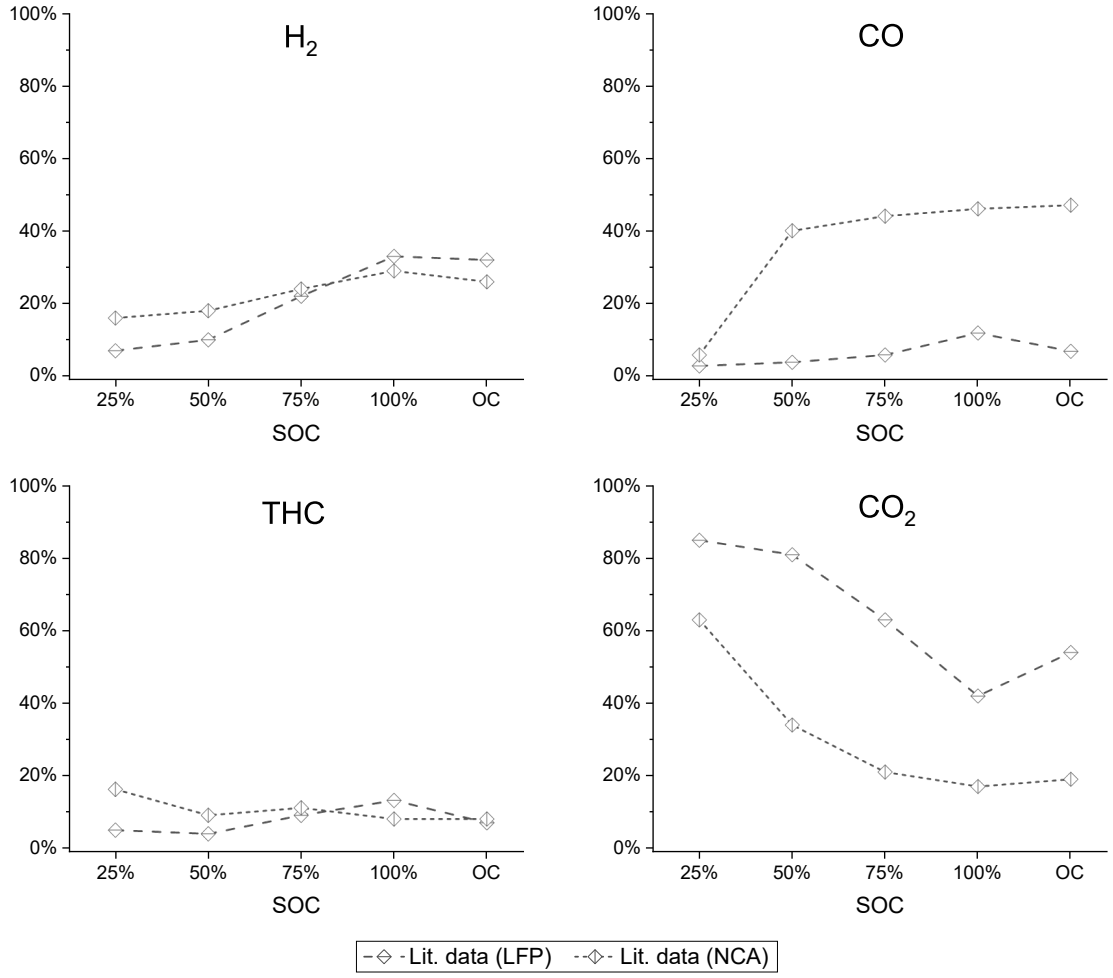

Figure 3. Mean concentrations of H_2, CO, CO_2 and THC in TR vent gas in inert atmosphere for two different cell chemistries, from literature (references are found in [10]); OC means overcharge.

For tests in air atmosphere, the gas composition may deviate from the results obtained in inert atmosphere since the vented gases may react with surrounding oxygen. Assuming that no major combustion (flames) occurs, the results are still similar, as seen in Figure 4 [2]. However, due to partial combustion, one can note a slight decrease in fraction of flammable gases such as CO and H2, and an increase in CO2. This is at least true for NMC which typically exhibit a greater risk of self-ignition than LFP due to higher maximum temperatures and ejection of glowing particles during a more violent TR scenario.

© RISE Research Institutes of Sweden

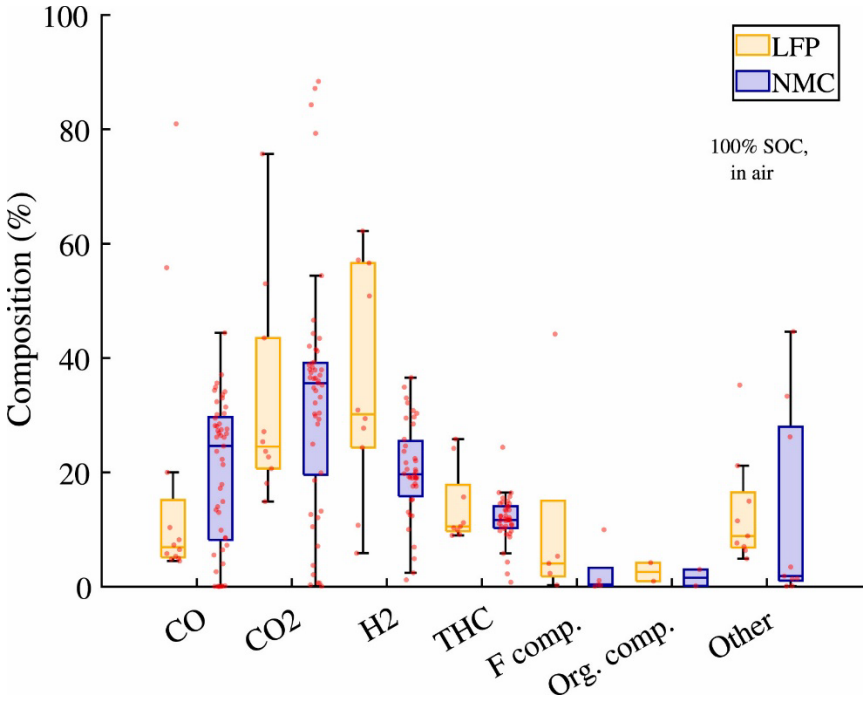

Figure 4. Gas composition for LFP and NMC cells at 100% SOC, venting in air atmosphere [2]

2.4 The effect of cell format

As with cell chemistry, variations in cell format can affect the gas production in terms of total battery vent gas emission. In the review performed by Bugryniec et al. [2], it was stated that prismatic cell formats tend to produce more battery vent gas and combustion gas (includes tests performed in both air and inert atmosphere) than pouch cells, followed by cylindrical cells. Larger form factors lead to lower heat loss per unit volume and thereby potentially increased temperatures. Increased temperature would lead to increased decomposition which may be the cause of the difference in battery vent gas production between cell format [2]. Contradictory, Rappsilber et al. [3] concluded in another review that pouch cells produce significantly higher gas emissions than prismatic cells, although it is not clear whether Rappsilber et al. include battery vent gas, combustion gas or both. However, in both studies it was concluded that pouch cells and prismatic cells produce more battery vent gas and/or combustion gas than cylindrical cells. Looking further into the gas composition, pouch cells tend to produce more CO and HF than other cell formats, but other than that, no distinctive trends in gas composition between cell formats has been found in the literature.

2.5 The effect of cell capacity

Comparing batteries of the same chemistry, 100% SOC and the same test atmosphere (inert/air), the total battery vent gas volume released during TR generally increases linearly with increased capacity [2]. This means that normalized battery vent gas volume (L/Wh) shows no increasing trends based on increased capacity. Most cell chemistries range within 1-3 L/Ah [2], [13], which allows for a degree of predictability of maximum battery vent gas volume. Not much data is available on the vent gas volume in the early stages, before TR, and no conclusions can be drawn on the impact from cell capacity or any other parameter.

© RISE Research Institutes of Sweden

The gas composition produced during TR has been reported to vary with cell capacity. As the capacity increases, the ratio of CO_2 decreases while CO increases. This shift in gas composition could be caused by uneven temperatures within larger batteries, hindering the complete reaction between O_2 and CO [12].

2.6 The effect of state of charge

The state of charge (SOC) will influence both the total gas volume and gas composition. An increase in SOC will increase the volume fractions of H_2 and CO and decrease the volume fraction of CO_2 [13], [20], see Figure 1 and Figure 3.

Moreover, an increase in the SOC tends to increase the volume of gas produced during TR [2], [10], [21]. This could be explained by the reactivity of the active material which is dependent on electrode potential [10], [21]. For LFP cells, which have lower electrode potentials and a flatter voltage profile, this trend is less evident as seen in Figure 5. The rate at which the gases are produced (i.e. gas release rate) is also increased as the SOC increases [10].

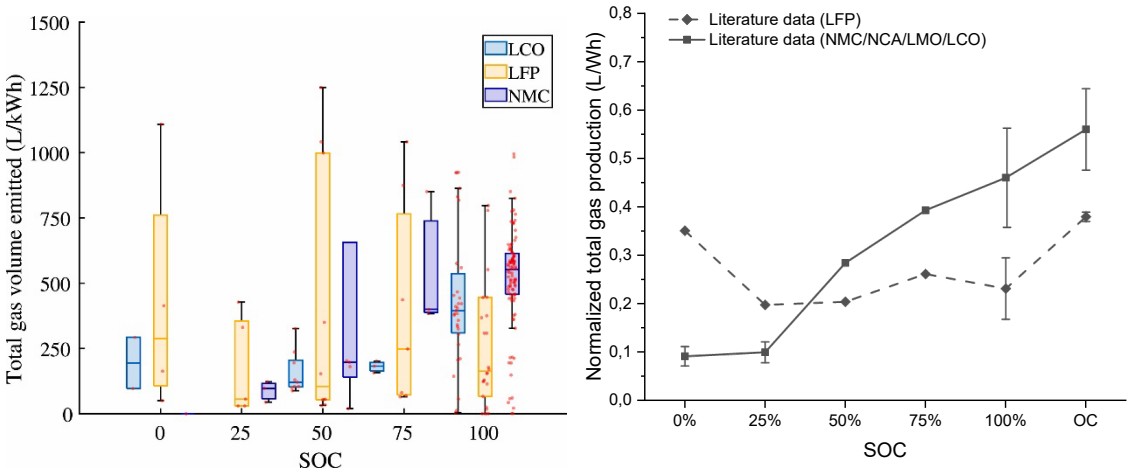

Figure 5. Literature data on the normalized battery vent gas volume (L/Wh) for tests in air and inert atmosphere (left) [2] and tests in inert atmosphere only (right) [13].

2.7 The effect of TR trigger method

Compared to other trigger methods, overcharge generally leads to an increase in the gas volume produced [10], [22], [23]. This is reasonable because it follows the effect of increased SOC and can be attributed to both the addition of energy into the battery cell and increased instability of the active materials [22], [23]. Due to increased instability of the cathode material and oxidation of the electrolyte at the cathode, overcharge may also lead to increased ratio of CO_2 [24].

For a fixed SOC level, different TR trigger methods have limited impact on the total gas volume produced but could have a large impact on the gas release rate [10]. In addition, different trigger methods will simulate different event scenarios and as pointed out before, a slow heating scenario may result in a first venting of the cell minutes before TR is triggered.

© RISE Research Institutes of Sweden

2.8 The effect of cell aging

There are inconclusive results in literature regarding the effect of cell aging on gas composition and volume from TR events. However, one effect is that aged cells have lower remaining capacity, which could result in lower gas generation [25]. This will be an effect of both lower maximum SOC and the consumption of electrolyte in the aging process.

2.9 Conclusions on gas composition and volume

Previous reviews reveal large variations in the reported gas volumes [L/kWh] and compositions during TR events. NMC cells tend to generate higher gas volumes than LFP cells. Moreover, high state of charge generally leads to higher gas volumes due to increased available energy. The same principle goes for overcharge as trigger method, where the additional added energy tends to increase the volume of produced gases during TR. The gas composition is generally dominated by H_2, CO, CO_2, volatile organic compounds and hydrocarbons, with proportions varying based on TR trigger method, temperature, SOC, cathode composition (notably nickel content) and if the tests were conducted in air or inert atmosphere. Variation in test methodologies, and challenges in distinguishing between vent gases and combustion products, underlines the need for standardized protocols (e.g., UL 9540A) and controlled environments to ensure comparability. However, the variating outcomes of battery abuse tests will also be present in real incidents, which features the importance to fully understand the capabilities and limitations of available detection methods.

© RISE Research Institutes of Sweden

3 Gas sensors

Chemical sensors are designed to selectively and reversibly respond to specific analytes, such as hydrogen or carbon monoxide, or groups of analytes, like flammable gases and volatile organic compounds (VOCs). These sensors have become increasingly important in various fields, including environmental monitoring, industrial process control, gas composition analysis, medicine, national defence, and public safety.

Chemical gas sensors are widely used to monitor air quality, particularly for ozone, nitric oxides, and carbon monoxide. Sensing technology is crucial for the safe and efficient use of hydrogen and biogas in different applications. Hydrogen sensors, for example, help prevent the accumulation of hydrogen to flammable levels by triggering alarms and activating safety measures.

Each type of sensor has its own strengths and weaknesses in terms of performance. For any application, the sensor must meet the specific needs of the end-user, which must be clearly identified and documented. To determine if a sensor meets the required specifications, its performance is evaluated based on various metrological criteria, also known as metrics. These criteria include accuracy, baseline, cross-sensitivity or selectivity, drift, final indication, hysteresis, limit of quantification, linear range/measuring range, noise, environmental effects (such as temperature, pressure, vibration, dust, and relative humidity), uncertainty, response/recovery time, reversibility, resolution, saturation, and sensitivity. These metrics are assessed within defined operational ranges of temperature, pressure, and relative humidity.

3.1 Performance assessments of gas sensors (metrics)

3.1.1 Precision

Precision refers to the degree of closeness between repeated measurements and is quantified by the standard deviation of these results. It can be categorized into repeatability, intermediate reproducibility, and reproducibility. Repeatability measures the consistency of measurements taken by the same instrument or individual under identical conditions, while intermediate reproducibility evaluates the consistency of measurements under varying conditions, such as different times, different operators, or different equipment, but within the same laboratory. Reproducibility, on the other hand, assesses the ability to replicate an entire study or experiment across different laboratories, with different operators, and using different equipment.

3.1.2 Trueness

Trueness refers to how closely a measured value aligns with the true value of the quantity being measured (measurand). When manufacturers list the specifications of sensors or analyzers, they often use the term "accuracy" to describe trueness.

© RISE Research Institutes of Sweden

3.1.3 Accuracy

Measurement accuracy describes how close a single measurement result is to the true quantity value and therefore includes the effect of both precision and trueness.

3.1.4 Response time

Response time refers to the speed at which a sensor reacts to a change in the input signal, typically measured in seconds. This time can vary based on test conditions, such as the calibration gas flow rate and ambient temperature. To measure response time, the gas concentration is altered, and the sensor output is monitored as the concentration increases or decreases. In the sensors industry, the response time T90 is commonly used. It represents the time required for the sensor to reach 90% of the target gas concentration or its stable reading. Conversely, the recovery time T10 is defined as the time it takes for the sensor to return to its baseline value after the measured variable is removed. This is usually specified as the time needed to fall to 10% of the final value after the step removal of the measured variable.

3.1.5 Stability and drift

Drift refers to the gradual change in an instrument's response to a constant concentration over time. This indicates that the performance of the measuring instrument is altering, necessitating re-calibration. Drift is typically caused by the aging of the sensor, but it can also result from factors such as dust accumulation and variations in pressure, temperature, and humidity. Overall, managing and mitigating drift is essential to ensure the accuracy and reliability of measurement instruments.

3.1.6 Selectivity/cross-sensitivity

Sensors are designed to selectively detect specific compounds or types of compounds. However, the presence of non-target compounds can sometimes produce a signal, leading to measurement errors for the target compound. This phenomenon, known as cross-sensitivity, can cause the signal for the target compound to be either higher or lower than expected. Manufacturers may provide a list of common gases and their typical effects on the sensor's signal at given concentrations to help mitigate this issue.

3.1.7 Limit of quantification and limit of detection

The limit of detection (LOD) represents the smallest amount of a substance that can be reliably detected, but not necessarily quantified, by an analytical procedure. It is the point at which the signal produced by the substance is distinguishable from the background noise with reasonable certainty.

The limit of quantification (LOQ), on the other hand, is the lowest concentration of a substance that can be quantitatively measured with acceptable precision and accuracy. It is the point at which the signal is not only detectable but also reliable enough to be used for precise quantification.

© RISE Research Institutes of Sweden

3.1.8 Nominal range, saturation

The nominal range is a common specification for sensors, indicating the range within which the sensor outputs exhibit the best linearity.Saturation occurs when the signal to be measured exceeds the sensor's dynamic range. In this state, the sensor's output reaches its maximum limit, causing a discrepancy between the true value and the measured value. This results in measurement errors.

3.1.9 Resolution

Resolution refers to the smallest detectable change in the input parameter that can be observed in the output signal. This means that the sensor can distinguish very fine differences in the measured quantity. Resolution is crucial for applications requiring high precision, as it determines the sensor's ability to detect small variations.

3.1.10 Hysteresis

A sensor should be capable of following the changes of the input parameter regardless of which direction the change is made; hysteresis is the measure of this property.

3.1.11 Reversibility

Reversibility refers to a sensor's capability to recover to its original baseline condition after being exposed to a target gas (analyte).

3.2 Test methods and test procedures

3.2.1 Flow through method

In the flow-through testing method, sensors are exposed to a continuous and controlled flow of test gas delivered through a gas line. This setup ensures that the sensors encounter the correct gas composition, which is crucial for accurate testing and calibration. The method allows for the simultaneous testing of multiple sensors, either in parallel or in series. Testing in series is particularly important for sensors that consume the component they measure, as it ensures each sensor receives the appropriate gas concentration.

One of the primary challenges of this method is maintaining a leak-proof interface between the sensors and the gas supply line. Any leaks can compromise the integrity of the test by allowing external air to mix with the test gas, leading to inaccurate results. Therefore, ensuring a secure and airtight connection is essential.

Another significant challenge is the precise control of environmental parameters such as humidity, pressure, and temperature. These factors can greatly influence sensor performance, and any variations can affect the reliability of the test results. Advanced control systems are often employed to maintain these parameters within strict limits.

While flow-through test methods are highly effective for evaluating sensors with very fast response times, they may not accurately simulate ambient conditions. In real-world applications, sensors often need to react to still air or airflow generated by ventilation systems. Flow-through methods, which rely on a continuous gas flow, might not

© RISE Research Institutes of Sweden

replicate these conditions accurately. However, they provide a controlled environment that is beneficial for specific testing scenarios.

Additionally, rapid flushing of the interface line before measurements is crucial to remove any residual gases that could affect the test results. Applying coatings from the gas intake point to the sensor can further minimize the risk of unwanted absorption of test substances. This is particularly important for ensuring that the gas reaching the sensor is pure and uncontaminated. Related process equipment, such as mass flow controllers (MFC) and valves, must also be carefully managed to prevent any absorption or contamination.

3.2.2 Chamber method

In the "chamber test" method, sensors are placed within a chamber designed to simulate flow-through conditions. This setup allows for precise control over environmental parameters such as humidity, temperature, and pressure. The pressure inside the chamber can be adjusted using a back pressure regulator and a vacuum pump, ensuring accurate simulation of various conditions.

Gas transport to the sensor in this method is primarily governed by diffusion, which closely mimics the sensor's deployment in real-world scenarios like rooms or other confined spaces. This diffusion-based transport is crucial for evaluating the sensor's performance in environments where airflow is minimal or controlled, such as indoor settings.

The capacity of the chamber determines the number of sensors that can be tested simultaneously. Larger chambers can accommodate more sensors, allowing for parallel testing and comparison under identical conditions.

3.2.3 Test procedures

To meaningfully test sensors, testing must be done according to testing protocols, preferably standardized. These protocols define performance requirements and test methods to assess that the metrics fulfil the requirements. However, this may prove to be challenging due to the lack of standard testing protocols, metrics, or targets to evaluate the performance of sensors for air matrix uniformly.

EPA just produces a technical report containing testing protocols, metrics, and target value for ozone air sensors which contains two parts: a base testing (in the field) and enhanced testing (in the laboratory) [26].

ATSM WK64899 “New Practice for Performance Evaluation of Ambient Air Quality Sensors and Other Sensor-Based Instruments” is under development within this ASTM Committee D22 (Air Quality). This standard intends to establish standardized tests and assessment criteria for the performance evaluation of sensor-based continuous instruments for ambient air quality measurements.

For hydrogen sensors, ISO standard 26142:2010 defines the performance requirements and test methods of hydrogen detection apparatus that is designed to measure and monitor hydrogen concentrations in stationary applications. It is intended to cover situations where the user desires the ability to detect hydrogen leaks and monitor hydrogen concentrations relevant to safety, primarily for hydrogen detection apparatus

© RISE Research Institutes of Sweden

at vehicle refueling stations but also to other stationary installations. The standard is intended to be used for certification purposes. It contains general requirements about construction, labelling and marking, instruction manual and vibration. Finally, the standard describes the tests to perform to control the performance requirements.

The National Renewable Energy Laboratory (NREL) has developed a variety of test protocols to quantitatively assess the performance specifications for hydrogen sensors [27]which is similar to ISO 26142 but more rigorous. Specific protocols were developed for linear range, short-term stability and the impact of fluctuations in temperature (-20, 0, 25, 50 and 85 ºC), pressure (0.8 to 1.2 bar), relative humidity (25, 50 and 85%) and chemical environment (CO, NO_2, H_2S, CH_4, NH_3, CO_2). The test gases are generated from blending certified gas mixtures with synthetic air. Typical range is 0 to 2% hydrogen in air.

RISE together with DTU and NPL [28] developed a protocol to test hydrogen sensors as part of the Met4H2 project (2022-2025). The tests proposed here are based on ISO 26142 which defines the performance requirements and test methods of hydrogen detection devices designed to measure and monitor hydrogen concentrations in stationary applications and on the standard hydrogen test protocols for the NREL sensor testing laboratory together with considerations from the Eurachem guide - the fitness for purpose of analytical methods to fulfill metrological assessment of the performances.

3.3 Relevant applications

3.3.1 Battery electric vehicle

Because of the limited volume in EV battery packs, gas sensors offer strong potential to provide early detection of cell failure in BEVs. However, this same limited space also restricts the number of sensors that can be installed. A limited number of gas sensors in combination with other relevant detection methods for cell failure such as electrochemical impedance spectroscopy (EIS) and data from the BMS, is therefore often suggested as a more viable approach. Potentially less price-sensitive segment than cars would be electric machinery and heavy vehicles.

3.3.2 Parking structures

3.3.2.1 Parking garages

Parking garages often consist of large volumes with high airflow rates to ventilate vehicle exhaust gases. High airflows can also be induced by wind in open constructions. These conditions pose a challenge for gas sensing, as effectively monitoring such spaces would require a large number of sensors. This becomes problematic due to the relatively high cost of gas sensors compared to the smoke and heat detectors commonly used today.

© RISE Research Institutes of Sweden

3.3.2.2 Ship transport

In addition to the previously mentioned challenges, the ceiling geometry on ships often features large steel beams that create squared sections. This can pose an issue for sensor placement, as it may delay detection if sensors are not positioned in each section, which would require a substantial number of sensors. Furthermore, passenger ferries often have open or semi-open vehicle decks, where wind flow during voyage could have a substantial impact on the possibility of gas sensing.

3.3.3 Battery energy storage systems (BESS)

BESS has wide use with many different applications such as supporting the electric grid, storing solar energy, electric propulsion on ships, and as container rentals to supply construction sites or festivals with electricity.

The geometry of these spaces is often that of closed containers or rooms containing battery racks, typically divided into sections, which is favourable for gas sensors (as one sensor can be placed in each section). To cool the batteries, each pack is often ventilated, although the air changes per hour (ACH) may not be very high. Sensors could be placed near the exhausts, and due to the small volume, the distance to the exhaust would likely be negligible.

3.3.4 Shipping (containers)

Majority of batteries used in our society are shipped in containers classified as dangerous goods. Each ship could carry thousands of containers, although far from all would contain batteries. Nevertheless, sensors would have to be provided at low cost if they were to be placed in every dangerous goods container.

3.3.5 Small batteries such as electric bicycles

Utilization of sensors is not applicable for this application yet because of issues with placement and costs. A possible application would instead be installation of sensors in bicycle rooms in buildings.

3.4 Sensor technology – advantages/disadvantages for each sensor type

There are many gas sensors available or in development. Different sensor can have for example different sensitivity, selectivity, response time, and reliability, and also different sensor size, cost, and power consumption and the choice of sensor depends on the application. This section provides a brief overview of each sensor technology, along with their respective advantages and disadvantages.

© RISE Research Institutes of Sweden

3.4.1 Catalytic sensors

For nearly a century, catalytic sensors have been used to detect various flammable gases. The catalytic sensor typically consists of two beads: an active bead coated with a catalyst (usually platinum) and a reference bead without the catalytic coating. These beads are arranged in a Wheatstone bridge configuration and heated above 300°C. When exposed to a combustible gas and air mixture, gas molecules adsorb on the catalytic bead's surface, leading to a catalytic combustion reaction. This reaction causes oxidation of the gas, generating heat and changing the electrical resistance of the platinum beads. The resistance variation is correlated with the gas concentration and converted into an electrical signal to indicate the presence and concentration of the combustible gas [29]. There are two types of catalytic sensors: Pellistor and hot-wire catalytic sensors. Pellistor sensor as described above is the most widely used type of catalytic gas sensor and consists of two beads coated with a catalyst. Hot-wire catalytic sensor uses a fine wire coated with a catalyst instead of beads [30].

Advantages with catalytic sensors are their low detection limit and fast response time, they can detect many different flammable gases and are cost-effective. Disadvantages are that they cannot detect non-combustible or inert gases, requires oxygen in the gas mixture, some chemicals can poison or degrade the catalyst, accuracy can be affected by humidity and temperature, and they may require a warm-up period before providing accurate results [31]. These sensors are typically used to detect hydrogen concentrations from 0 to 4% [32].

3.4.2 Electrochemical sensors

The working principle of an electrochemical gas sensor involves several steps. The electrochemical cell structure consists of three key components: the working electrode, counter electrode, and reference electrode. The working electrode is coated with a specific chemical or catalyst to facilitate the reaction with the target gas. The counter electrode completes the circuit and usually consists of a noble metal like platinum. The reference electrode provides a stable reference potential for reliable measurements.

When the sensor is exposed to the target gas, the working electrode absorbs or adsorbs the gas molecules. This triggers an electrochemical reaction, specifically a redox reaction, which changes the cell's electrical properties. There are two main types of reactions: oxidation-reduction reactions, which involve the oxidation or reduction of gas molecules and change the current flow, and ion exchange reactions, which involve ion exchange in the electrolyte solution and affect voltage or current. The electrochemical reaction generates an electrical signal proportional to the gas concentration. To ensure accurate measurements, the sensor needs to be calibrated by relating the electrical signal to known gas concentrations. There are three types of electrochemical gas sensors: amperometric, potentiometric, and voltametric sensors. Amperometric sensors monitor the electric current generated from the electrochemical reaction, potentiometric sensors measure the potential difference between the working electrode and the reference electrode while voltametric sensors apply a time dependent potential to the working electrode and measure the resulting current as a function of that potential [33], [34].

© RISE Research Institutes of Sweden

Advantages with electrochemical sensors are their high sensitivity, high selectivity, their fast response time and their energy efficiency. The drawbacks are their limited lifespan, need for calibration and they are relatively expensive [31].

3.4.3 Resistance based sensors

3.4.3.1 Metal-oxide semiconductor (MOS) sensors

Since the 1950s, it has been known that the electrical properties of metal oxides change when exposed to reducing gases [35]. In 1962, Seiyama first applied this phenomenon to gas detection using a ZnO thin film [36].

The conductivity of semiconducting metal oxides changes based on the nature of the gas molecules (oxidizing or reducing) and the type of majority charge carriers (n-type or p-type). In n-type oxides, adsorbed oxygen molecules remove electrons from the conduction band, creating a potential barrier and increasing resistance. When reducing gases (donors) such as NH_3, H_2, and H_2S are present electrons are released, lowering the potential barrier and increasing conductivity. Conversely, oxidizing gases (acceptors) like O_3, NO, Cl_2 and NO_2 cause further electron loss, increasing the potential barrier and resistance [37]. For p-type oxides, the detection mechanism involves changes in resistance due to oxidation or reduction reactions with the target gas. At room temperature, adsorbed oxygen molecules capture conduction band electrons, forming oxygen ions and increasing the concentration of p-type carriers, which decreases resistance. Reducing gases cause electrons to recombine with holes, increasing resistance, while oxidizing gases increase hole concentration, decreasing resistance.

A significant shortcoming of semiconductor gas sensors is their low selectivity, as they are cross-sensitive to other reducing and hydrogen-containing compounds. They can become less accurate over time necessitating regular recalibrations and they can be influenced by humidity and high temperature. Advantages are that they have high sensitivity, low cost and fast response time.

3.4.3.2 Metallic resistor

The electrical resistivity of certain metals and alloys, particularly palladium, changes significantly upon absorbing hydrogen. These sensors detect hydrogen by measuring the increase in electrical resistivity due to the formation of palladium hydride. Typically, metallic resistor sensors are made by depositing a metal film on a substrate between two electrical contacts.

A hydrogen sensor using a thin film Pd-Ni alloy offers a wide measuring range of 0.1-100%, with Ni suppressing phase transitions in palladium and enhancing durability [38]. Another sensor uses a thin palladium-coated Mg-Ni alloy film for hydrogen detection in the range of 10 ppm to 10% at room temperature, with changes in resistance due to hydrogen absorption [39]. While selective to hydrogen, these sensors can be poisoned by gases like CO, SO_2, and H_2S, with sensor performance depending on the palladium film morphology.

A sensor with a discontinuous ultrathin palladium film on a siloxane-treated glass substrate has been developed. This sensor detects hydrogen based on the expansion of

© RISE Research Institutes of Sweden

nano-sized palladium particles, forming new electrical connections and decreasing resistance. This technology offers a rapid response time, a lower detection limit, and resistance to poisoning by CO, O2, and CH4 [40].

3.4.4 Mechanical sensors

When hydrogen is absorbed by a metal, it occupies interstitial sites in the metal lattice, causing the lattice to expand and altering the metal's physical properties. Micro-fabricated palladium-coated cantilevers use this expansion as the detection principle. These sensors have a palladium film coated on one side of a cantilever. The substrate on which the film is coated restricts volume expansion upon hydrogen absorption, causing induced stresses that lead to mechanical bending or curvature of the cantilever. Research on cantilever hydrogen sensors is limited, and one issue is the interfacial sliding, delamination, and detachment of the palladium film due to expansion/contraction weakening the palladium/substrate adhesion. The initial adhesion strength depends on the deposition method of the palladium film. Palladium films created by sputtering bombardment show superior adhesion and hydrogen detection characteristics due to efficient mechanical transduction. Enhancing Pd adhesion by fabricating trenches on the cantilever surface has improved hydrogen sensing down to 50 ppm and provided faster response times [41].

3.4.5 Optical sensors

Optical sensors measure variations in light using technologies like LEDs, lasers, optical fibers, and photodetectors. There are two types of optical sensors: colorimetric sensors, which use dyes that change colour in response to gases, and fluorescence sensors [42]. Advantages with optical sensors are their high selective, they have low detection limits (especially fluorescence sensors), and they can monitor a wide range of gases. Disadvantages are that performance can be compromised when exposed to gases they are not designed to detect, they can be affected by temperature, humidity, and pressure and they have short working range [31]. Below are some examples of optical sensor technologies.

3.4.5.1 Fiber optic sensors

Optical sensors rely on detecting changes in intensity, phase, frequency/wavelength, or polarization. Often the optical signal is sent through an optical fibre which can guide the light to the region of interest and has the added benefit of being insensitive to electromagnetic radiation, not needing an electrical signal, thus being spark free. Fiber optical gas sensors can be divided into two main categories, extrinsic and intrinsic. For extrinsic sensors the optical fibre is used to carry the light signal to a sensing chamber and from the sensing chamber to a detector. The detection of gases then relies on how the optical signal changes within the chamber depending on the gas content. In other words, the fibre is not an active sensor. For intrinsic sensors on the other hand the optical fibre itself is an active sensor. A transducer is added to the fibre that converts a change in the surrounding environment to a change in optical signal.

© RISE Research Institutes of Sweden

3.4.5.2 Surface plasmon resonance

Plasmonic sensors operate based on the influence of the surrounding medium on plasmon resonance. When molecules are absorbed on the surface of plasmonic nanoparticles, they cause a shift in the extinction peak, which serves as the sensor's descriptor. These sensors are widely used in various applications, particularly in biosensors for disease diagnosis, detecting biomolecules in wastewater, and gas sensors for monitoring air quality or detecting hydrogen [43], [44].

Plasmonic hydrogen sensors, which use palladium (Pd) or Pd-alloy nanoparticles, are notable for their selective, low detection limit and ultrafast response to hydrogen, detecting concentrations as low as a few hundred parts per billion. However, a significant drawback is their susceptibility to CO poisoning, as CO molecules in the air can block hydrogen dissociation on Pd surfaces, hindering hydrogen absorption into the Pd lattice [45].

3.4.6 Infrared sensors

When gas is present inside the sample chamber, the gas molecules interact with the infrared light emitted by the infrared source. This interaction occurs because the gas molecules absorb specific infrared wavelengths. The optical sensor's filter only allows the wavelength associated with the target gas to pass through. The amount of gas present can be determined because the number of photons absorbed is directly proportional to the energy of the photon beam from the emitter. This allows to calculate the concentration of the detected gas molecules [46].

These sensors offer several advantages, including high selectivity, which allows them to distinguish specific gases within complex mixtures, and high sensitivity, enabling the detection of even trace amounts. They also provide fast and accurate readings, making them suitable for real-time monitoring. However, infrared gas sensors also have limitations. They can only detect gases that absorb infrared light, excluding those without IR absorption bands (excluding H_2 for example). Additionally, their complex design can lead to higher manufacturing costs and require regular calibration and maintenance. Environmental factors such as temperature and humidity may also affect their accuracy, necessitating compensation mechanisms [31] [ref].

3.4.7 Acoustic sensors

Acoustic gas sensors operate based on how sound waves travel through a medium. The speed of sound in a gas is influenced by its density, viscosity, and composition. By monitoring changes in the speed of sound, the presence and concentration of specific gas components can be determined. These sensors typically consist of a transmitter, a receiver, and a gas cell containing the gas sample. The transmitter sends an acoustic signal through the gas, which is then received by the receiver. The time it takes for the sound wave to travel from the transmitter to the receiver, known as the time of flight (TOF), is affected by the gas composition. By analyzing the TOF data, the sensor can identify the type and concentration of the target gas.

© RISE Research Institutes of Sweden

Advantages of acoustic wave gas sensors are their high sensitivity, high selectivity and fast response time. Their drawbacks are their size and weight, they can be impacted by temperature and humidity, and they require calibration and maintenance [31].

3.4.8 Work function-based sensors

3.4.8.1 Schottky diode

Schottky-type sensors typically consist of a metal in contact with a semiconductor material or a metal in contact with a thin insulating layer (usually an oxide) on a semiconductor material. When a Schottky sensor is exposed to gases, a chemical reaction occurs with the metal oxide layer. The gas molecules dissociate and diffuse into the metal, forming a dipolar layer at the metal-semiconductor interface. These dipolar layers changes the metal work function and hence alter the Schottky barrier, either increasing or decreasing it, which in turn changes the current-voltage (I-V) characteristics. The response can be measured as a change in voltage when the diode is operated at constant bias current [31], [41].

Advantageous with these types of sensors is that they are highly sensitive to specific gases, they have a fast response time, they can be designed for excellent selectivity for specific gases and they can handle a broad temperature range. Disadvantages is that they are designed for specific gases, limiting versatility, they are sensitive to contaminants and humidity and they can give false positive to gas molecules that are similar to the one it is designed for.

3.4.8.2 Metal oxide semiconductor field transistor (MOSFET)

MISFET or MOSFET sensors are semiconductor sensors that use a field effect transistor (FET) to convert changes in the work function of a catalytic metal gate, due to gas presence, into an electrical signal indicating the concentration. Typically, these sensors consist of a metal (catalytic for the target gas)–SiO_2–Si triple layer structure. The Si substrate is ion-implanted to form a source and a drain. The catalytic metal, acting as the gate, is deposited on the insulating oxide layer. Grounding the source contact and applying a positive bias to the gate creates an inversion layer at the semiconductor surface, allowing current to flow between the source and drain. The specific gas detected depends on the catalytic properties of the metal used in the sensor's gate. But these sensors can detect hydrogen, nitrogen dioxide and other noxious gases [41], [47].

3.4.9 Thermal conductivity sensors

This technology includes two types of gas sensors. The first type is similar to a pellistor (rf. catalytic) and consists of two inert resistor beads with thermoresistors. One resistor, the detecting resistor, is exposed to the environment to detect gas, while the other, the reference resistor, is in a chamber with reference gas, usually air. These resistors are connected in a Wheatstone bridge circuit. When exposed to the same gas, they generate heat at the same rate, resulting in a zero reading. However, when the detecting resistor encounters the target gas, it loses heat based on the gas's thermal conductivity compared to the reference gas, causing temperature variations and resistance changes, which create an imbalance in the Wheatstone bridge.

© RISE Research Institutes of Sweden

The second type of sensor does not require a reference cell. It has two elements: a "hot" and a "cold" element with a constant temperature difference. Heat is transferred from the hot to the cold element through the target gas. The thermal conductivity of the target gas, related to its concentration, determines the power needed to maintain the hot element's temperature [41].

The advantages of thermal conductivity gas sensors are their high sensitivity, their long-term stability and robustness, they can detect a wide range of gases both flammable and non-flammable. Disadvantages are that they are sensitive to changes in the environment, consumes power and they may exhibit cross-sensitivity to different gases.

3.4.10 Polymer-based sensors

This technology is divided into conducting polymer and non-conducting polymer. Conducting polymers can act as electron donors or acceptors when they come into contact with gas molecules, altering the concentration of carriers and, consequently, the electrical conductivity or resistance of the sensing polymers [48], [49]. Non-conducting polymer-based gas sensors, also known as insulating polymer sensors, use non-conductive polymers as the sensing material. These sensors detect gases by monitoring changes in the polymer's properties, such as capacitance, resistance, or optical characteristics. When gas molecules interact with the polymer, the properties of the polymer change, which can then be measured and linked to the concentration or presence of the gas. For example, gas interaction can cause variations in the polymer layer's thickness or dielectric constant, modifying its capacitance. The polymer may also swell or contract due to gas molecules, affecting its resistance. Additionally, gas molecules can alter the polymer's optical properties, such as fluorescence, reflection, and absorption. By detecting these changes, the sensor can determine the concentration and presence of the gas [50], [51].

Polymer-based gas sensors offer several advantages, including cost-effectiveness, low power consumption, customizability for specific gas detection, fast response time, and compact design. However, they also have disadvantages such as long-term instability of some polymer materials, limited selectivity and sensitivity compared to other sensor types, they need regular calibration and can be affected by environmental factors like temperature and humidity, which can affect accuracy [31].

3.5 Conclusions on gas sensors

Each type of sensor has its own performance strengths and weaknesses. For any application, it is crucial that the sensor meets the specific needs of the end-user, which should be clearly identified. Each sensor technology offers unique advantages and disadvantages and can be selected based on specific requirements such as its performance for detecting specific gases associated with TR and the intended placement of the sensor (see Figure 6 for a summary of the different sensor technologies and their advantages and disadvantages).

© RISE Research Institutes of Sweden

To determine whether a sensor meets the required specifications, its performance is rigorously evaluated based on various metrological criteria, also known as metrics. These criteria include accuracy, baseline, cross-sensitivity or selectivity, drift, final indication, hysteresis, limit of quantification, linear range/measuring range, noise, environmental effects (such as temperature, pressure, vibration, dust, and relative humidity), uncertainty, response/recovery time, reversibility, resolution, saturation, and sensitivity.

Figure 6. Different sensor techniques and their advantages and disadvantages.

© RISE Research Institutes of Sweden

4 Electrochemical impedance spectroscopy

Electrochemical impedance spectroscopy (EIS) is a widely used, non-destructive technique for characterization of batteries and can be used as a diagnostic or prognostic tool throughout the battery lifetime [52]. EIS can be used for state estimation such as for State-of-Charge (SOC) and State-of-Health (SOH), as well as internal temperature estimation [53] which is of vital importance for early detection of TR. Some research [54], [55] indicate that EIS is a promising technique for specifically early detection of TR, as it has shown to provide quicker response and earlier indications of failure, venting and temperature increase compared to only thermocouples and gas sensors.

EIS is operated in either galvanostatic or potentiostatic mode, where a sinusoidal current or voltage respectively is applied with a certain amplitude and frequency. The corresponding response in terms of amplitude and phase shift of the output voltage or current is then measured. To obtain a complete impedance spectra, this is repeated for a number of frequencies in a predefined frequency range. The resulting output is represented in either a Nyquist or Bode plot. An example of a Nyquist plot for a LIB is shown in Figure 7 [52], the spectrum is divided into high-, intermediate-, and low frequency range. The frequency is increasing towards the left in the plot.

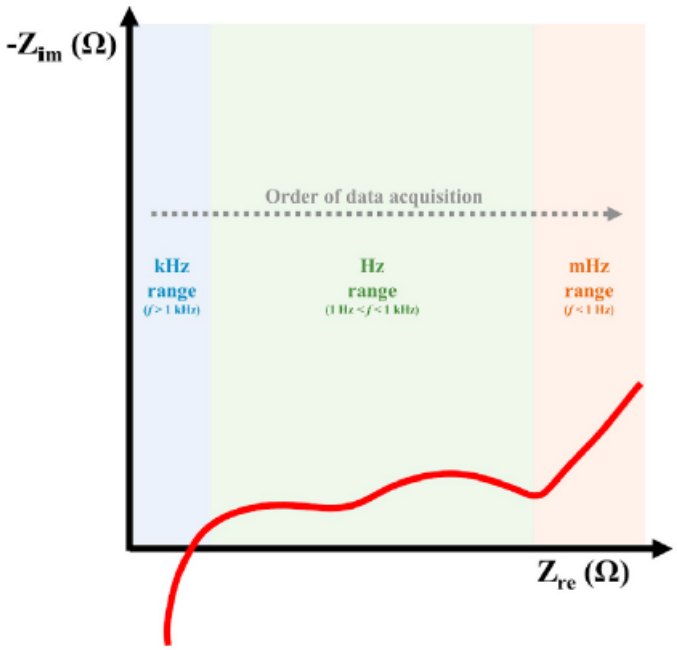

Figure 7. Schematic example of Nyquist plot for a LIB. The negative imaginary part of impedance is plotted against the real part of the impedance. Frequency is increasing to the left in the plot, data is normally obtained with decreasing frequency.

© RISE Research Institutes of Sweden

4.1 EIS for early detection of thermal runaway

As previously mentioned, EIS is a strong tool for battery characterization and the characteristics of the EIS spectra changes with SOC, SOH, temperature and battery chemistry, to mention some examples. This means that through mapping of the EIS spectra with varying SOC, SOH and temperature, it is possible to track the progression and behavior of the battery and use EIS for state estimations and temperature monitoring. However, different segments of the EIS spectra, i.e. different frequencies, are dependent on the different parameters [56]. To use EIS as an efficient tool for evaluation of battery status, it is critical to identify frequency ranges that show a strong dependency towards the parameter under evaluation and low or no dependency towards other parameters. In the case for early detection of failures and TR, it is thus vital to identify which parts of the frequency range that has a strong dependency on temperature, but low or no dependency on SOC or SOH.

Li et al. [53] evaluated four features from the EIS spectra, real part of impedance (Z'), imaginary part of impedance (Z"), absolute value of impedance (|Z|) and the phase angle (θ), and investigated their connection to temperature and their potential for TR detection. They concluded that for an NMC cell, the parameters from the medium-high frequency range (28.6 Hz-7.1 kHz) had a more pronounced contribution to the prediction of temperature. For LFP cells, the corresponding frequency range was found to be the high range (>1kHz). In more detail, they found that, for NMC, θ at 1 kHz had the lowest sensitivity to SOC and high sensitivity to temperature. Additionally, |Z| at around 1 kHz showed low sensitivity to SOC while moderate sensitivity to temperature meaning that this frequency is suitable for temperature predictions and early detection of TR.

Several other studies [55], [56], [57], [58] have shown similar results where the phase angle of the impedance generally in the range of 10-1000 Hz is the feature that show strongest temperature dependence while low SOC or SOH dependence, both for LFP and NMC cells. Srinivasan et al [58] claim that cathode chemistry does not affect the impedance at frequencies above 30 Hz. Considering phase angle as feature for cell temperature prediction and early detection of TR, this would imply a straightforward methodology as only one measurement point is required. Table 3 summarizes the frequency ranges and features that can be linked to temperature prognostics for different cell chemistries, according to the references studied in the literature review.

© RISE Research Institutes of Sweden

Table 3. Frequency range and feature linked to temperature prognostics for different cell chemistries, according to the listed studies.

Study	Cell chemistry	Frequency range	Feature
Li et. al. [53]	NMC	1 kHz	θ, |Z|
	LFP	>1 kHz	θ, Z"
Carkhuff et. al. [55]	Not specified	10-200 Hz	θ
Bhoir et. al. [56]	NMC	520-640 Hz	θ
Dong et. al. [57]	NMC	30-500 Hz	θ
	NCA		
Srinivasan et. al. [58]	LCO	40-100 Hz	θ
	LFP		
	Not specified		

4.1.1 Use of EIS in battery systems and real applications

Research is being conducted in order to find the linkage between the different features, and frequency range of the impedance spectra of batteries and the cell temperature but in order to make EIS an accessible tool for the early detection of TR it must be realized in real battery systems and show potential for BMS implementation. One example is Torres-Castro et al [54] that used rapid EIS in combination with gas sensors for early detection of failures and TR. They identified markers from both EIS data and gas sensor data corresponding to onset of failure and these markers can then become part of the BMS for monitoring and avoiding critical scenarios. They used as feature the magnitude of the impedance, i.e. |Z|, and for failure marker the first point of increasing magnitude after a minimum. The experiments were carried out on NMC pouch cells, both on cell level and multicell configurations in series and parallel, in overtemperature and overcharge abuse until TR. They found that for overtemperature abuse rapid EIS gave up to three times longer warning time compared to gas sensors and for overcharge abuse rapid EIS gave similar warning times as gas sensors.

Another example is the BITS-BMS, battery internal temperature sensor-based BMS, developed by Charkuff et al [55]. It is a low-power, multifrequency impedance-based BMS capable of monitoring both amplitude and phase shift. A regular BMS might not be able to detect mismatched cells adequately which could lead to significant battery failure. They show that via impedance it is possible to make a more accurate comparison between cells and therefore better match cells and enable cell balancing, while monitoring the internal temperature.

© RISE Research Institutes of Sweden

4.1.2 Advantages and disadvantages with EIS for early detection of thermal runaway

The use of EIS in battery prognostics allows for more accurate and rapid response on specifically temperature increase compared to only gas sensors and thermocouples, at the same time as it opens up for better determination of cell matching and balancing. Furthermore, EIS can be used not only for early detection of failures but can also be used for state estimations, such as SOC and SOH, although not described in detail in this review. However, one drawback of EIS is that the measurements normally require a system at steady state to provide the most accurate results and to avoid harmonics that can be interpreted as noise, this means EIS become time consuming and therefore unpractical for the use in battery systems [54], [55]. To overcome this, rapid data collection over a wider frequency range, or data collection from a narrower frequency range, is crucial. Combination of EIS with other sensor techniques, such as gas sensors and temperature sensors, would give the best chances for early detection of battery failure and TR.

© RISE Research Institutes of Sweden

5 Review on thermal runaway detection tests

This chapter summarizes previous tests that have been conducted with focus on early detection of TR in Li-ion batteries. There exist some articles and reviews discussing early detection of TR based mainly on theoretical assumptions, e.g. focusing on various heat detection methods [59] or gas detection methods [60]. However, the focus here is on actual tests that have been performed that include a TR scenario. A further delimitation made to the study was to only include tests involving more than one type of sensor. Information about the test setups, test methodologies and test results are important background information for the design of the experimental test plan within the project.

5.1 Single cell tests

Several studies have reported single cell tests. With focus on early detection, tests with single cells are relevant since TR likely starts in one cell and detection is demanded before propagation to adjacent cells. However, single cell tests are also limited in representing a real scenario regarding the interaction with surrounding cells, the venting strategy of a battery system, and the possible relative positions of the cell and sensor. Depending on the detection technology and placement of the detector, the setup could be more or less realistic as compared to a real scenario.

5.1.1 Dahlbom et al. (2023)

In this study [61] 14 tests were performed, all of which were conducted at cell-level and at 50% SOC. The study evaluated combined smoke and heat detectors (point type), CO detectors (point type), lower explosion-limit detector (point type), thermal imaging camera, light detection and ranging (LIDAR) system and video analytics.

5.1.1.1 Test setup

Several test setups and test scenarios were utilized, having the cell positioned in the open, inside an ISO container, or covered by a small hood, all in air atmosphere, see Figure 8. Most tests were conducted addressing TR in a battery cell, but some tests were also conducted addressing a conventional fire scenario using wood sticks on a hot plate (EN 54).

© RISE Research Institutes of Sweden

Figure 8. Tests performed in the open, inside an ISO container, and with a cell covered by a small hood.

5.1.1.2 Conclusions

Detection in a small and confined volume is relatively easy, but detection in a large space or in the open is a greater challenge. If the gases are cooled, they sink and spread along the floor as seen in the right photo in Figure 8Figure 8. Shielding may be a problem, especially with LIDAR and thermal imaging. It was concluded that the buoyancy of gases was not fully understood and that large-scale tests would be needed to validate the conclusions drawn from the cell-level tests. In future work, it was recommended that the SOC is varied and that other types of gas detectors are evaluated.

5.1.2 Cai et al. (2021)

A large part of this paper [62] discusses TR detection based on previous tests and associated gas analysis data, before presenting some new tests conducted. The conclusion from the review of tests was that carbon dioxide detection is a viable option. The tests conducted were therefore focused on CO_2 detection, but voltage, temperature, and force sensors were also included.

5.1.2.1 Test setup

The test setup is shown in Figure 9. The acrylic box had small openings to avoid pressure build-up. All sensors were positioned inside the box. The cell was overcharged to trigger TR.

© RISE Research Institutes of Sweden

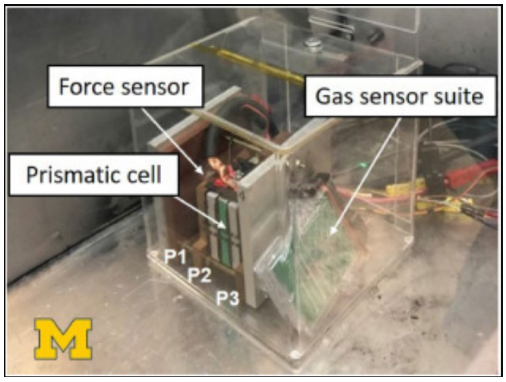

Figure 9. Test setup with a prismatic cell positioned in an aluminum fixture inside an acrylic box.

5.1.2.2 Conclusions

The experiment demonstrated the effectiveness of CO_2 detection upon gas venting from a single cell. However, the experiment also showed that the force sensor, temperature sensors and voltage sensor could detect abnormalities before gas venting.

5.1.3 Essl et al. (2021)

This work [63] investigates four different failure cases with gas emissions: unwanted electrolysis (e.g. liquid coolant or condensed water), vaporizing electrolyte, first venting, and TR. More than 30 TR experiments were conducted using four different cell types, utilizing both overcharge, overtemperature and nail-penetration scenarios. Several gas sensors were tested including different sensor manufacturers and sensor principles.

5.1.3.1 Test setup

The test setup was a closed pressure vessel with inert N_2 atmosphere, see Figure 10. The vaporizing electrolyte scenario was done with two different electrolyte mixtures without any other cell components. Overcharge and over-temperature scenarios resulted in gas release from first venting in the order of minutes before TR, while the nail penetration scenario resulted in an immediate TR.

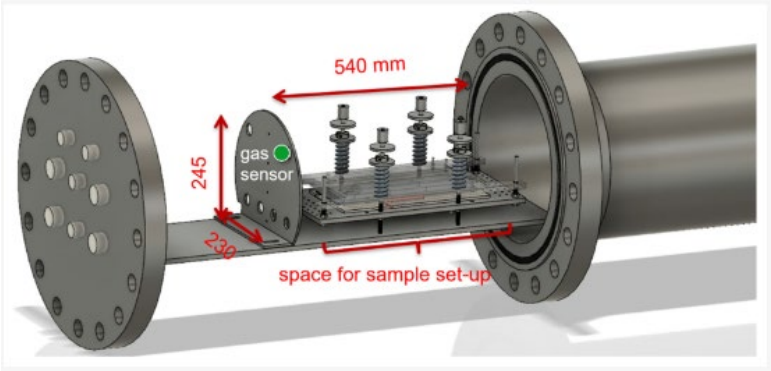

Figure 10. Test setup with the cell positioned in a stainless-steel pressure vessel with inert atmosphere.

© RISE Research Institutes of Sweden

5.1.3.2 Conclusions

Based on the performed tests, detectability is summarized in Figure 11 for the different sensor principles for the tested failure cases. However, also sensor lifetime and cross sensitivity are pointed out as important parameters when choosing the most suitable sensor. It is recommended that a combination of different monitoring techniques as well as several gas sensors are used in the battery pack for fast and reliable detection of all scenarios and to overcome some of the challenges regarding cross sensitivity and reliability.

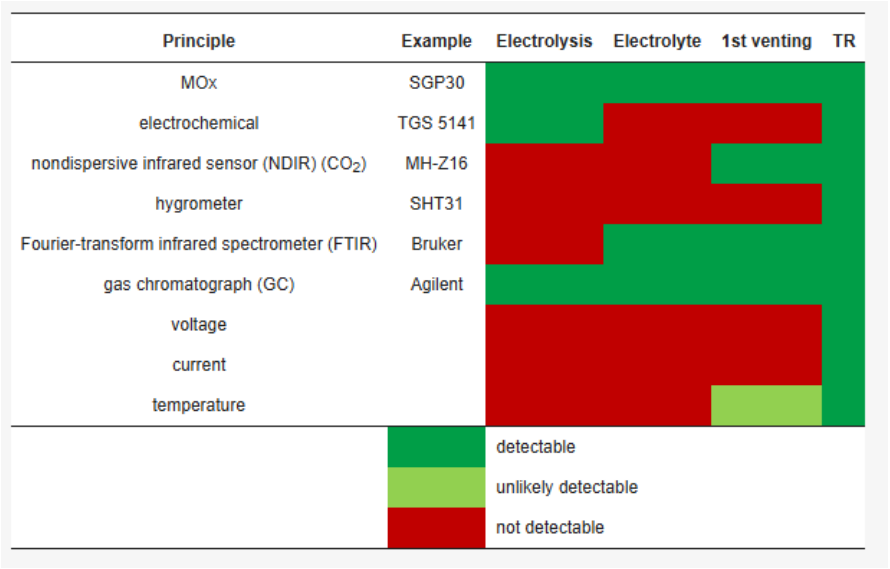

Figure 11. Conclusions on the detectability for the tested sensors and failure cases.

5.1.4 Malmquist (2024)

This is a hands-on investigation [64] of different smoke and gas sensors' ability to detect LIB off-gas during a TR scenario. The cylindrical LIB cell was triggered by a slow heating scenario generating first venting ahead of TR. Evaluated sensors included a VOC detector, an aspirating cloud chamber detector, a CO (10 ppm) detector, an optical smoke detector, and a "domestic" CO detector (~400 ppm).

5.1.4.1 Test setup

The cylindrical cell was positioned such that vented gases were collected in a small box, see Figure 12. Only the top part of the battery cell is seen.

© RISE Research Institutes of Sweden

Figure 12. Test setup where the cell (red arrow) ventilates gases inside a transparent box.

5.1.4.2 Conclusions

Starting from first venting, the quickest detection was achieved by the VOC detector, followed by the aspirating cloud chamber detector, CO (10 ppm) detector, optical smoke detector, and last the "domestic" CO (400 ppm) detector. In these tests, the time from first venting to TR was in the order of 10-15 minutes with detection by the different sensors spread over this interval.

5.1.5 Yang et al. (2024)

TR warning experiments were conducted using H2, CO, CO2, CH4, and smoke gas sensors during nail penetration of cylindrical and hard-shell LFP batteries at various SOCs [65].

5.1.5.1 Test setup

Tests were conducted inside a small box (no dimensions presented), see Figure 13. Nail penetration tests were conducted at 25%, 50%, 75%, and 100% SOC.

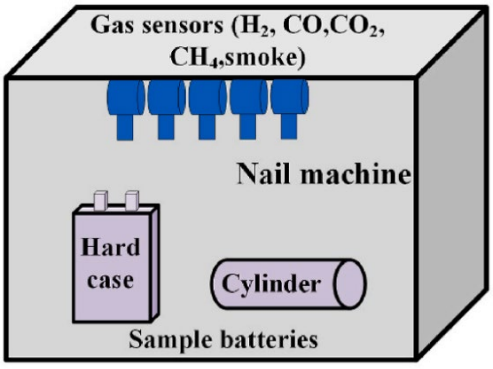

Figure 13. Test setup where the cell is triggered by nail penetration inside a small box. Gas sensors are positioned inside the box.

5.1.5.2 Conclusions

Among the monitored gases, H_2 gas was detected earlier than others followed by CO and then the other three. However, there were some variations between the tests and

© RISE Research Institutes of Sweden

the largest difference between sensors was 20 s, while the time interval from nail penetration to detection was within 74 s in all tests. Time interval decreased with increasing SOC due to sooner ventilation of gases.

5.1.6 Internal cell pressure

Both Cheng et al. [66], Lai et al. [67], and Wei et al. [68] have shown that early warning can be achieved based on cell internal pressure measurements in overtemperature and overcharge scenarios. Either in advance of voltage and temperature failure detection, or in combination with these for robustness and reliability. Lin et al. [69] showed that during venting of a cell in overcharge, nail penetration, and external heating scenarios, distinct expansion force signals occur earlier than corresponding voltage and temperature signals.

5.2 Multiple cells or system level tests

5.2.1 Torres-Castro et al. (2024)

This study [54] investigates the use of electrochemical impedance spectroscopy (EIS) and gas sensing technology for early warning of TR. Three gas sensors were evaluated: a volatile organic compound (VOC) gas detector, an H_2 sensor, and a combined VOC, CO_2, and H_2 sensor. 12 Ah NMC pouch cells at 100% SOC were used, either as single cells or in module configurations. TR was triggered by either overtemperature (5 °C/min ramp) or overcharge scenarios.

5.2.1.1 Test setup

The cells were put together between fixture plates and put into an open box inside a room, seen in Figure 14. The distance between battery and sensor #5 in the figure was 2 meters (7 feet). Comparison of different sensing technologies were done at the position of sensor #2.

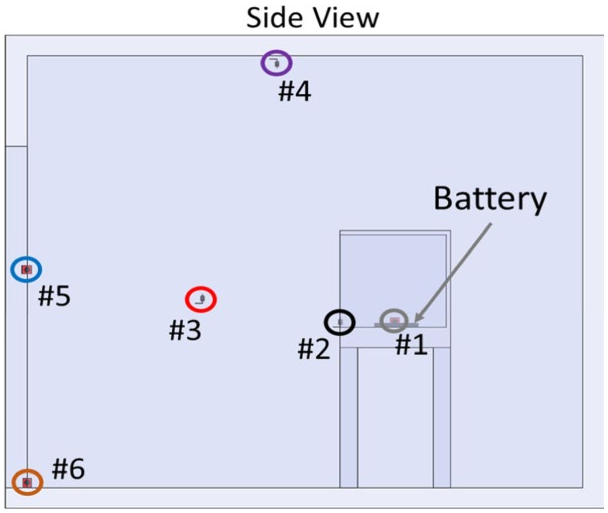

Figure 14. Side view of the room test setup, where the placement of 6 VOC detectors is indicated; the difference in detection time between these sensors was maximum 36 seconds.

© RISE Research Institutes of Sweden

5.2.1.2 Conclusions

For the overtemperature tests, rapid EIS detection was followed by VOC sensors, with H_2 sensors showing the shortest warning time. For overcharge tests, EIS detection and VOC sensors were comparable and gave warning at first venting, while the H_2 sensor in most cases did not trigger until an occurring TR.

5.2.2 Barowy et al. (2021)

Three fire tests were conducted with batteries inside an ISO container [70]. Different detectors were positioned in different positions in the container including detection of CO, H_2, smoke, and combustible gases (LEL detector).

5.2.2.1 Test setup

The three tests were performed inside an ISO container with identical battery configuration, including several battery modules, each containing thirty 18650 cylindrical cells at 100% SOC, see Figure 15. TR was triggered in one cylindrical cell using a flexible film heater.

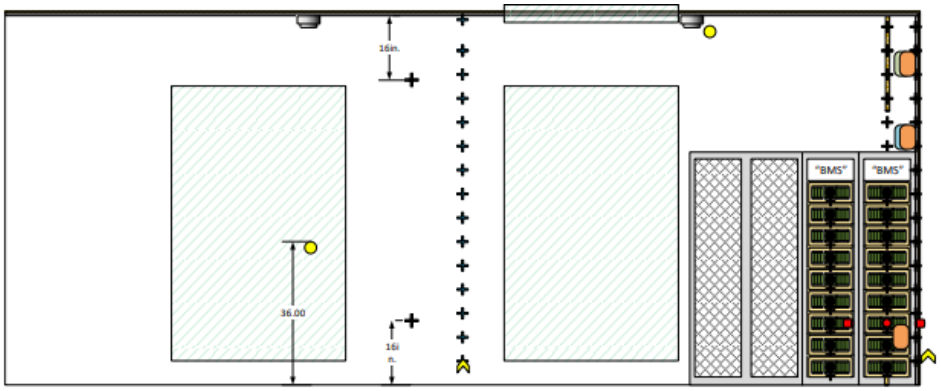

Figure 15. Side view of the container test setup. Smoke detectors are positioned in the roof and gas detectors are positioned on the side wall at different heights indicated by orange markings.

5.2.2.2 Conclusions

All detectors gave alarm within a minute from the TR event. CO, H_2 and combustible gas detectors were faster than the smoke detectors, but detector position and proximity to the initiating cell was the most important factor. Hydrogen was detected in the first test, but problems with the detector in the following tests made evaluation of the detection time difficult.

The tested gas detectors were effective to indicate that a TR event had occurred but were not reliable for an ongoing assessment of hazard conditions.

5.2.3 Koch et al. (2018)

The aim of this study [71] was to evaluate different sensors' abilities to quickly detect a TR inside a battery pack. Seven types of sensors were tested including measurements of cell voltage, gas (CO, CH_4, and C_3H_8), smoke, pollution (electrical resistivity on a circuit board, creep distance), temperature, gas pressure and force between cells. Three tests were conducted with pouch cells at 100% SOC.

© RISE Research Institutes of Sweden

5.2.3.1 Test setup

The three tests included a single cell, one module, and two modules, respectively, which were encapsulated inside an aluminium housing with venting openings. In the single cell test, TR was triggered by a heater, while nail penetration was utilized in the module tests.

5.2.3.2 Conclusions

The results showed that all the tested sensors were able to detect a TR when positioned inside a battery pack. However, they received different ratings based on detection speed, signal clarity and sensor feasibility, see Figure 16.

Sensor	Detection Speed	Signal Clarity	Sensor Feasibility
S1 voltage	-	+	+
S2 gas	+	+	-
S3 smoke	-	0	0
S4 creep distance	-	-	+
S5 temperature	0	0	0
S6 pressure	+	-	+
S7 force	+	-	0

Figure 16. Conclusions for the different sensors evaluated. Detection speed describes how fast a TR can be detected, signal clarity describes how close the detection signal comes to a step function and how easy it is to evaluate, and sensor feasibility evaluates how easily the sensor can be deployed. The grading goes from (+) good, to (0) neutral to (-) bad.

5.2.4 Choi et al. (2025)

Early detection was investigated for three fully charged cells connected in parallel (suppression tests also included module and pack configurations) [72]. TR was triggered by heating (7 °C/min). Temperature and voltage were monitored at cell level and a VOC gas sensor was detecting gases above the cells.

5.2.4.1 Test setup

Experiments were performed inside a large test chamber (20 m height and 20 m diameter). The VOC sensor was positioned 0.2 m above the battery.

5.2.4.2 Conclusions

Temperature and VOC concentration monitoring were found to be effective for identifying abnormal battery conditions prior to TR onset. Noticeable increase in VOC concentrations was detected at a cell surface temperature of approximately 240 °C, about 4 min before TR.

© RISE Research Institutes of Sweden

5.3 Conclusions on early detection tests

A summary of the reviewed detection tests is presented in Table 4. Early warning prior to cell TR can be achieved in slow temperature increase scenarios, for example when the cell is heated slowly or overcharged. Voltage, temperature, and cell internal pressure sensors and algorithms may detect failures before first venting in such scenarios. At first venting, VOC detectors have performed well. CO_2 detectors and very sensitive gas or smoke analysers have also been able to detect these gases.

Most sensors and detectors can detect TR after initiation. For a fast failure scenario, for example due to internal short circuit, TR may occur within seconds from initial local temperature increase. Some tests show that gases such as H_2 and CO can be detected earliest in such scenarios, before e.g. temperature and voltage failure detection.

It is important to point out that gas detection in a small and confined place, such as inside a battery pack or module, is relatively easy. Detection in the open or in a large space is a greater challenge. Depending on cell type, battery design, and SOC, the temperature and composition, and thereby the buoyancy of gases, can be very different from case to case.

© RISE Research Institutes of Sweden

Table 4. Summary of previously conducted experiments with detection of TR.

Author et. al	1. Confined/open 2. Trigger method 3. Inert/air	Detection methods	Conclusion
Dahlbom, 2023	1. Both 2. Slow heating 3. Air	Smoke & heat, CO sensor, LEL sensor, thermal imaging, LIDAR, video analytics	Detection in small, confined volumes is manageable, shielding is an issue for LIDAR and thermal imaging, buoyancy of gases not fully understood
Cai, 2021	1. Small confined 2. Overcharge 3. Air	CO_2 sensor, force sensor, voltage, temperature,	CO_2 sensor was effective. Force, temperature and voltage sensor could all detect abnormalities before first venting.
Essl, 2021	1. Small confined 2. Overcharge, slow heating, nail penetration 3. Inert	VOC&CO_2 sensor, CO sensor, NDIR, hygrometer, FTIR, GC, voltage, current, temperature	Metal oxide VOC&CO_2 sensor could detect all stages of TR.
Malmquist, 2024	1. Small confined 2. Slow heating 3. Air	VOC sensor, aspirating cloud chamber detector, CO sensor, optical smoke detector, domestic CO detector	VOC sensor had shortest time to detection. Domestic CO detector had longest time to detection
Yang, 2024	1. Small confined 2. Nail penetration 3. Air	H_2, CO, CO_2, CH_4 sensors, smoke detector	Good performance of all sensors. H2 sensor had shortest time to detection
Torres-Castro, 2024	1. Large confined 2. Slow heating, overcharge 3. Air	VOC sensor, H2 sensor, Combined VOC/CO_2/H_2 sensor	Rapid EIS and VOC sensor had shortest time to detection
Barowy, 2021	1. Large confined 2. Slow heating 3. Air	Smoke, CO sensor, H_2 sensor, LEL sensor	Good performance of all sensors. Location of sensor more important than type.
Koch, 2018	1. Small confined 2. Rapid heating 3. Air	Voltage, gas (CO/CH_4/C_3H_8), smoke, creep distance, temperature, pressure, force	Gas, pressure and force had shortest time to detection
Choi, 2025	1. Open 2. Slow heating 3. Air	Voltage, temperature, VOC sensor	Temperature and VOC sensor could detect well before TR onset.

© RISE Research Institutes of Sweden

6 References

[1] "2024 Annual Battery Report." Accessed: Apr. 15, 2025. [Online]. Available: https://volta.foundation/battery-report-2024

[2] P. J. Bugryniec, E. G. Resendiz, S. M. Nwophoke, S. Khanna, C. James, and S. F. Brown, "Review of gas emissions from lithium-ion battery thermal runaway failure — Considering toxic and flammable compounds," *J Energy Storage*, vol. 87, p. 111288, May 2024, doi: 10.1016/J.EST.2024.111288.

[3] T. Rappsilber *et al.*, "Meta-analysis of heat release and smoke gas emission during thermal runaway of lithium-ion batteries," *J Energy Storage*, vol. 60, p. 106579, Apr. 2023, doi: 10.1016/J.EST.2022.106579.

[4] E. J. K. Nilsson and A. Ahlberg Tidblad, "Gas Emissions from Lithium-Ion Batteries: A Review of Experimental Results and Methodologies," *Batteries 2024, Vol. 10, Page 443*, vol. 10, no. 12, p. 443, Dec. 2024, doi: 10.3390/BATTERIES10120443.

[5] "UL 9540A Test Method for Battery Energy Storage Systems (BESS) | UL Solutions." Accessed: May 26, 2025. [Online]. Available: https://www.ul.com/services/ul-9540a-test-method

[6] J. Weng *et al.*, "Alleviation on battery thermal runaway propagation: Effects of oxygen level and dilution gas," *J Power Sources*, vol. 509, p. 230340, Oct. 2021, doi: 10.1016/J.JPOWSOUR.2021.230340.

[7] Y. Zhu *et al.*, "Critical conditions for the thermal runaway propagation of lithium-ion batteries in air and argon environments," *J Therm Anal Calorim*, vol. 147, no. 23, pp. 13699–13710, Dec. 2022, doi: 10.1007/S10973-022-11575-2/FIGURES/10.

[8] Y. Yang *et al.*, "Carbon oxides emissions from lithium-ion batteries under thermal runaway from measurements and predictive model," *J Energy Storage*, vol. 33, p. 101863, Jan. 2021, doi: 10.1016/J.EST.2020.101863.

[9] H. Wang *et al.*, "Fire and explosion characteristics of vent gas from lithium-ion batteries after thermal runaway: A comparative study," *eTransportation*, vol. 13, p. 100190, Aug. 2022, doi: 10.1016/J.ETRAN.2022.100190.

[10] O. Willstrand, M. Pushp, P. Andersson, and D. Brandell, "Impact of different Li-ion cell test conditions on thermal runaway characteristics and gas release measurements," *J Energy Storage*, vol. 68, p. 107785, Sep. 2023, doi: 10.1016/J.EST.2023.107785.

[11] C. Di Bari *et al.*, "Recent safety focused overall analysis, testing and accident reviews towards safer e-mobility and energy storage".

[12] B. Nie, Y. Dong, and L. Chang, "The evolution of thermal runaway parameters of lithium-ion batteries under different abuse conditions: A review," *J Energy Storage*, vol. 96, p. 112624, Aug. 2024, doi: 10.1016/J.EST.2024.112624.

© RISE Research Institutes of Sweden

[13] O. Willstrand, J. Hynynen, A. Karlsson, and D. Brandell, “Gas release from lithium-ion batteries and mitigation of potential consequences,” in *Proceedings of the 15th International Symposium on Hazards, Prevention and Mitigation of Industrial Explosions (ISHPMIE 2024)*, 2024, pp. 137–148. doi: 10.5281/ZENODO.12621001.

[14] G. Wei *et al.*, “A comprehensive insight into the thermal runaway issues in the view of lithium-ion battery intrinsic safety performance and venting gas explosion hazards,” *Appl Energy*, vol. 349, p. 121651, Nov. 2023, doi: 10.1016/J.APENERGY.2023.121651.

[15] C. Misiewicz, “Probing the Gaseous Phase in Batteries Big and Small,” p. 2457, 2024, Accessed: Apr. 15, 2025. [Online]. Available: http://urn.kb.se/resolve?urn=urn:nbn:se:uu:diva-539865

[16] M. Yang *et al.*, “A comprehensive study of thermal runaway behavior and early warning subjected to internal short-circuit,” *J Power Sources*, vol. 620, p. 235213, Nov. 2024, doi: 10.1016/J.JPOWSOUR.2024.235213.

[17] Y. Fernandes, A. Bry, and S. de Persis, “Identification and quantification of gases emitted during abuse tests by overcharge of a commercial Li-ion battery,” *J Power Sources*, vol. 389, pp. 106–119, Jun. 2018, doi: 10.1016/J.JPOWSOUR.2018.03.034.

[18] C. F. Larsson, “Lithium-ion Battery Safety - Assessment by Abuse Testing, Fluoride Gas Emissions and Fire Propagation,” 2017, Accessed: Apr. 15, 2025. [Online]. Available: https://research.chalmers.se/en/publication/251352

[19] H. Shen *et al.*, “Thermal Runaway Characteristics and Gas Composition Analysis of Lithium-Ion Batteries with Different LFP and NCM Cathode Materials under Inert Atmosphere,” *Electronics 2023, Vol. 12, Page 1603*, vol. 12, no. 7, p. 1603, Mar. 2023, doi: 10.3390/ELECTRONICS12071603.

[20] A. R. Baird, E. J. Archibald, K. C. Marr, and O. A. Ezekoye, “Explosion hazards from lithium-ion battery vent gas,” *J Power Sources*, vol. 446, p. 227257, Jan. 2020, doi: 10.1016/J.JPOWSOUR.2019.227257.

[21] T. Shan, P. Zhang, Z. Wang, and X. Zhu, “Insights into extreme thermal runaway scenarios of lithium-ion batteries fire and explosion: A critical review,” *J Energy Storage*, vol. 88, p. 111532, May 2024, doi: 10.1016/J.EST.2024.111532.

[22] C. Essl, A. Golubkov, and A. Fuchs, “Comparing Different Thermal Runaway Triggers for Two Automotive Lithium-Ion Battery Cell Types,” *J Electrochem Soc*, vol. 167, no. 13, p. 130542, Oct. 2020, doi: 10.1149/1945-7111/ABBE5A.

[23] C. Xu *et al.*, “A comparative study of the venting gas of lithium-ion batteries during thermal runaway triggered by various methods,” *Cell Rep Phys Sci*, vol. 4, no. 12, p. 101705, Dec. 2023, doi: 10.1016/J.XCRP.2023.101705.

[24] T. Ohsaki *et al.*, “Overcharge reaction of lithium-ion batteries,” *J Power Sources*, vol. 146, no. 1–2, pp. 97–100, Aug. 2005, doi: 10.1016/J.JPOWSOUR.2005.03.105.

© RISE Research Institutes of Sweden

[25] F. Larsson, S. Bertilsson, M. Furlani, I. Albinsson, and B. E. Mellander, “Gas explosions and thermal runaways during external heating abuse of commercial lithium-ion graphite-LiCoO2 cells at different levels of ageing,” *J Power Sources*, vol. 373, pp. 220–231, Jan. 2018, doi: 10.1016/J.JPOWSOUR.2017.10.085.

[26] R. Duvall, A. Clements, G. Hagle, A. Kamal, and V. Kilaru, “Performance Testing Protocols, Metrics, and Target Values for Ozone Air Sensors,” Washington, DC, USA, 2021.

[27] W. Buttner, “Standard Hydrogen Test Protocols for the NREL Sensor Testing Laboratory (Brochure), NREL (National Renewable Energy Laboratory),” 2011. [Online]. Available: http://www.nrel.gov/hydrogen/pdfs/42987.pdf

[28] “A 1.3.2. PROTOCOL FOR TESTING HYDROGEN SENSORS - Met4h2.” Accessed: Apr. 16, 2025. [Online]. Available: https://met4h2.eu/news-and-publications/a-1-3-2-protocol-for-testing-hydrogen-sensors/

[29] “Catalytic type - Operating principle - Technology - FIGARO Engineering inc.” Accessed: Apr. 15, 2025. [Online]. Available: https://www.figaro.co.jp/en/technicalinfo/principle/catalytic-type.html

[30] X. Liu, S. Cheng, H. Liu, S. Hu, D. Zhang, and H. Ning, “A Survey on Gas Sensing Technology,” *Sensors 2012, Vol. 12, Pages 9635-9665*, vol. 12, no. 7, pp. 9635–9665, Jul. 2012, doi: 10.3390/S120709635.

[31] S. Panda, S. Mehlawat, N. Dhariwal, A. Sanger, and A. Kumar, “Comprehensive review on gas sensors: Unveiling recent developments and addressing challenges,” *Materials Science and Engineering: B*, vol. 308, p. 117616, Oct. 2024, doi: 10.1016/J.MSEB.2024.117616.

[32] K. Ashhar, Y. Cui, L. J. Kuehsamy, D. W. Y. Khoo, and F. M. Kai, “A survey of sensor testing methods for hydrogen leakage detection and purity analysis,” *Measurement: Sensors*, p. 101714, Feb. 2025, doi: 10.1016/J.MEASEN.2024.101714.

[33] K. Chen, W. Chou, L. Liu, Y. Cui, P. Xue, and M. Jia, “Electrochemical Sensors Fabricated by Electrospinning Technology: An Overview,” *Sensors 2019, Vol. 19, Page 3676*, vol. 19, no. 17, p. 3676, Aug. 2019, doi: 10.3390/S19173676.

[34] S. Capone *et al.*, “SOLID STATE GAS SENSORS: STATE OF THE ART AND FUTURE ACTIVITIES,” *Journal of Optoelectronics and Advanced Materials*, vol. 5, no. 5, pp. 1335–1348, 2003.

[35] C. Wagner, “The Mechanism of the Decomposition of Nitrous Oxide on Zinc Oxide as Catalyst,” *J Chem Phys*, vol. 18, no. 1, pp. 69–71, Jan. 1950, doi: 10.1063/1.1747459.

[36] T. Seiyama, A. Kato, K. Fujiishi, and M. Nagatani, “A New Detector for Gaseous Components Using Semiconductive Thin Films,” *Anal Chem*, vol. 34, no. 11, pp. 1502–1503, 1962, doi: 10.1021/AC60191A001/ASSET/AC60191A001.FP.PNG_V03.

© RISE Research Institutes of Sweden

[37] N. Nasiri and C. Clarke, “Nanostructured Chemiresistive Gas Sensors for Medical Applications,” *Sensors 2019, Vol. 19, Page 462*, vol. 19, no. 3, p. 462, Jan. 2019, doi: 10.3390/S19030462.

[38] R. C. Hughes and W. K. Schubert, “Thin films of Pd/Ni alloys for detection of high hydrogen concentrations,” *J Appl Phys*, vol. 71, no. 1, pp. 542–544, Jan. 1992, doi: 10.1063/1.350646.

[39] K. Yoshimura *et al.*, “New hydrogen sensor based on sputtered Mg–Ni alloy thin film,” *Vacuum*, vol. 83, no. 3, pp. 699–702, Oct. 2008, doi: 10.1016/J.VACUUM.2008.04.047.

[40] T. Xu *et al.*, “Self-assembled monolayer-enhanced hydrogen sensing with ultrathin palladium films,” 2031, doi: 10.1063/1.1929075.

[41] T. Hübert, L. Boon-Brett, G. Black, and U. Banach, “Hydrogen sensors – A review,” *Sens Actuators B Chem*, vol. 157, no. 2, pp. 329–352, Oct. 2011, doi: 10.1016/J.SNB.2011.04.070.

[42] A. D. Wilson and M. Baietto, “Applications and Advances in Electronic-Nose Technologies,” *Sensors 2009, Vol. 9, Pages 5099-5148*, vol. 9, no. 7, pp. 5099–5148, Jun. 2009, doi: 10.3390/S90705099.

[43] J. N. Anker, W. P. Hall, O. Lyandres, N. C. Shah, J. Zhao, and R. P. Van Duyne, “Biosensing with plasmonic nanosensors,” *Nature Materials 2008 7:6*, vol. 7, no. 6, pp. 442–453, Jun. 2008, doi: 10.1038/nmat2162.

[44] B. Špačková, P. Wrobel, M. Bocková, and J. Homola, “Optical Biosensors Based on Plasmonic Nanostructures: A Review,” *Proceedings of the IEEE*, vol. 104, no. 12, pp. 2380–2408, Dec. 2016, doi: 10.1109/JPROC.2016.2624340.

[45] I. ¨ Ostergren *et al.*, “A surface passivated fluorinated polymer nanocomposite for carbon monoxide resistant plasmonic hydrogen sensing A surface passivated fluorinated polymer nanocomposite for carbon monoxide resistant plasmonic hydrogen sensing †,” 2024, doi: 10.1039/d4ta00055b.

[46] S. Esfahani, A. Tiele, S. O. Agbroko, and J. A. Covington, “Development of a Tuneable NDIR Optical Electronic Nose,” *Sensors 2020, Vol. 20, Page 6875*, vol. 20, no. 23, p. 6875, Dec. 2020, doi: 10.3390/S20236875.

[47] Y. Jeong *et al.*, “NO2 Sensing Characteristics of Si MOSFET Gas Sensor Based on Thickness of WO3 Sensing Layer,” *Journal of Sensor Science and Technology*, vol. 29, no. 1, pp. 14–18, Jan. 2020, doi: 10.5369/JSST.2019.29.1.14.

[48] X. Liu, W. Zheng, R. Kumar, M. Kumar, and J. Zhang, “Conducting polymer-based nanostructures for gas sensors,” *Coord Chem Rev*, vol. 462, p. 214517, Jul. 2022, doi: 10.1016/J.CCR.2022.214517.

[49] A. Verma, R. Gupta, A. S. Verma, and T. Kumar, “A review of composite conducting polymer-based sensors for detection of industrial waste gases,” *Sensors and Actuators Reports*, vol. 5, p. 100143, Jun. 2023, doi: 10.1016/J.SNR.2023.100143.

© RISE Research Institutes of Sweden

[50] L. Gao *et al.*, “Ultrasensitive flexible NO2 gas sensors via multilayer porous polymer film,” *Sens Actuators B Chem*, vol. 368, p. 132113, Oct. 2022, doi: 10.1016/J.SNB.2022.132113.

[51] Y. Zhu *et al.*, “Bilayer polymer dielectric systems for high response NO2 gas sensors,” *Mater Lett*, vol. 288, p. 129370, Apr. 2021, doi: 10.1016/J.MATLET.2021.129370.

[52] N. Meddings *et al.*, “Application of electrochemical impedance spectroscopy to commercial Li-ion cells: A review,” *J Power Sources*, vol. 480, no. May, 2020, doi: 10.1016/j.jpowsour.2020.228742.

[53] Y. Li *et al.*, “Early warning method for thermal runaway of lithium-ion batteries under thermal abuse condition based on online electrochemical impedance monitoring,” *Journal of Energy Chemistry*, vol. 92, pp. 74–86, 2024, doi: 10.1016/j.jechem.2023.12.049.

[54] L. Torres-Castro, A. M. Bates, N. B. Johnson, G. Quintana, and L. Gray, “Early Detection of Li-Ion Battery Thermal Runaway Using Commercial Diagnostic Technologies,” *J Electrochem Soc*, vol. 171, no. 2, p. 020520, 2024, doi: 10.1149/1945-7111/ad2440.

[55] B. G. Carkhuff, P. A. Demirev, and R. Srinivasan, “Impedance-Based Battery Management System for Safety Monitoring of Lithium-Ion Batteries,” *IEEE Transactions on Industrial Electronics*, vol. 65, no. 8, pp. 6497–6504, 2018, doi: 10.1109/TIE.2017.2786199.

[56] S. Bhoir, G. Thenaisie, and M. Paolone, “Li-ion Battery Internal Temperature Estimation using Electrochemical Impedance Spectroscopy,” *2023 International Conference on Clean Electrical Power, ICCEP 2023*, pp. 13–19, 2023, doi: 10.1109/ICCEP57914.2023.10247457.

[57] P. Dong, Z. Liu, P. Wu, Z. Li, Z. Wang, and J. Zhang, “Reliable and Early Warning of Lithium-Ion Battery Thermal Runaway Based on Electrochemical Impedance Spectrum,” *J Electrochem Soc*, vol. 168, no. 9, p. 090529, 2021, doi: 10.1149/1945-7111/ac239b.

[58] R. Srinivasan, B. G. Carkhuff, M. H. Butler, and A. C. Baisden, “Instantaneous measurement of the internal temperature in lithium-ion rechargeable cells,” *Electrochim Acta*, vol. 56, no. 17, pp. 6198–6204, 2011, doi: 10.1016/j.electacta.2011.03.136.

[59] L. H. J. Raijmakers, D. L. Danilov, R. A. Eichel, and P. H. L. Notten, “A review on various temperature-indication methods for Li-ion batteries,” *Appl Energy*, vol. 240, pp. 918–945, Apr. 2019, doi: 10.1016/J.APENERGY.2019.02.078.

[60] Z. Liao, S. Zhang, K. Li, G. Zhang, and T. G. Habetler, “A survey of methods for monitoring and detecting thermal runaway of lithium-ion batteries,” *J Power Sources*, vol. 436, p. 226879, Oct. 2019, doi: 10.1016/J.JPOWSOUR.2019.226879.

[61] “Horizon 2020 Project acronym: LASH FIRE Project full title: Legislative Assessment for Safety Hazard of Fire and Innovations in Ro-ro ship

© RISE Research Institutes of Sweden

Environment Evaluation of Detection Principles and Challenges in Early Detection of Thermal Runaway in Batteries," 2019.

[62] T. Cai, P. Valecha, V. Tran, B. Engle, A. Stefanopoulou, and J. Siegel, "Detection of Li-ion battery failure and venting with Carbon Dioxide sensors," *eTransportation*, vol. 7, p. 100100, Feb. 2021, doi: 10.1016/J.ETRAN.2020.100100.

[63] C. Essl, L. Seifert, M. Rabe, and A. Fuchs, "Early Detection of Failing Automotive Batteries Using Gas Sensors," *Batteries 2021, Vol. 7, Page 25*, vol. 7, no. 2, p. 25, Apr. 2021, doi: 10.3390/BATTERIES7020025.

[64] "Detektera batteribränder, visst går det - YouTube." Accessed: Apr. 15, 2025. [Online]. Available: https://www.youtube.com/watch?v=UAhtx0TdtBQ

[65] M. Yang *et al.*, "A comprehensive study of thermal runaway behavior and early warning subjected to internal short-circuit," *J Power Sources*, vol. 620, p. 235213, Nov. 2024, doi: 10.1016/J.JPOWSOUR.2024.235213.

[66] Z. Cheng *et al.*, "Early warning of thermal runaway for larger-format lithium iron-phosphate battery by coupling internal pressure and temperature," *Appl Energy*, vol. 383, p. 125396, Apr. 2025, doi: 10.1016/J.APENERGY.2025.125396.

[67] X. Lai *et al.*, "Enhancing early warning systems: Experimental investigation of physical signals in thermal runaway evolution of large-capacity lithium iron phosphate batteries," *J Power Sources*, vol. 632, p. 236389, Mar. 2025, doi: 10.1016/J.JPOWSOUR.2025.236389.

[68] S. Wei *et al.*, "Study on Thermal Runaway Behavior and Early Warning Algorithm of Ternary Lithium Battery Pack Under Preload Force," *Energy Technology*, vol. 12, no. 12, p. 2401238, Dec. 2024, doi: 10.1002/ENTE.202401238.

[69] C. Lin *et al.*, "Early warning for thermal runaway of Li [Ni0.5Co0.2Mn0.3] O2 and LiFePO4 batteries under external heating, penetration and overcharging conditions," *J Energy Storage*, vol. 109, p. 115085, Feb. 2025, doi: 10.1016/J.EST.2024.115085.

[70] A. Barowy, A. Klieger, J. Regan, and M. Mckinnon, "UL 9540A Installation Level Tests with Outdoor Lithium-ion Energy Storage System Mockups," 2021.

[71] S. Koch, K. P. Birke, and R. Kuhn, "Fast Thermal Runaway Detection for Lithium-Ion Cells in Large Scale Traction Batteries," *Batteries 2018, Vol. 4, Page 16*, vol. 4, no. 2, p. 16, Mar. 2018, doi: 10.3390/BATTERIES4020016.

[72] S. Choi *et al.*, "Early Detection and Suppression of Thermal Runaway in Large-Format Lithium-Ion Batteries: Insights from Experimental Analysis," 2025, doi: 10.3390/en18010155.

© RISE Research Institutes of Sweden

Appendix 2: Gas sensors evaluation tests

Authors: Karine Arrhenius, Lesly Paradina

1 Introduction

The composition and flammability of the gases released during thermal runaway (TR) events vary depending on diverse conditions as it has been shown in the literature review.

Chemical sensors play a crucial role in preventing flammable gas accumulation by triggering alarms and activating safety systems. However, it is essential to assess their performance independently and metrologically to ensure their reliable and accurate measurement.

Each sensor has its own advantages and disadvantages in terms of performance and operational conditions. Therefore, sensor needs to be chosen for a specific application depending not only on the ambient working conditions but also on the detection requirements and sensor performance capabilities. In each application, a sensor's ability to perform the measurements must meet the end-user needs which must be identified and documented. Hence, that research contributes to a deeper understanding of sensor performance in hazardous environments and support the development of safer battery energy systems.

This report presents results from the sensor evaluation tests. The main goal of this task is to evaluate the performance of different detection technologies for early identification of TR events in lithium-ion batteries (LIBs).

2 Methodology

The experimental plan for assessment of sensors was established in the project. For evaluation of sensors, RISE have a test rig developed and designed for testing of different types of sensors used in the hydrogen supply chain, and capable of measuring most of the metrics under different operating conditions. Operating conditions such as temperature, humidity, gas composition, gas concentrations etc. can be varied. The main metrological criteria for sensors were evaluated, including trueness and response time (T90) / recovery time (T10).

2.1 Sensors

Three sensors with different kind of technologies were evaluated: Molecular Property Spectrometer™ (MPS™) technology, Nanoplasmonic (NPS) technology and a sensor based on AI predictions.

The MPS sensor is capable to detect flammable gases, and its response is related to Lower Explosive Limit (LEL %) that refers to the minimum concentration of a

© RISE Research Institutes of Sweden

flammable gas or vapor in air that can ignite and cause combustion. According to the manufacturer, this MPS technology allows the sensor to detect and quantify multiple flammable gases using a single sensor configuration, offering real-time measurement of gases from 0 to 199 % LEL.

The second sensor uses NPS technology and detects H_2. NPS is an optical, versatile technology that detects hydrogen also in the absence of oxygen. The sensors have palladium alloy nanostructure transducers. In the presence of hydrogen, the optical signature of the nanostructures changes, generating the sensor signal. The sensor signal is reversible and corresponds to the partial pressure of hydrogen in the sensor chip environment. Its nanoplasmonic sensor element reacts quickly and selectively to hydrogen also in the absence of oxygen. NPS is still a technology under development, and it is worth noticing that palladium alloys used in this technology are known to be affected by carbon-oxide species.

The third sensor is an AI prediction sensor. This technology combines advanced sensor technology with Internet of Things (IoT) solutions. The sensor is based on changes in electrical resistance and temperature, that are used in training models to predict the presence of pollutants in air. The signal response is detected or not detected pollutants/gas of interest in air.

2.2 Rig operating conditions/parameters

The tested sensors were prepared and mounted in a manner representative of the typical application, in accordance with the instruction or operation manual. There are at least two distinct methods to test sensors, the “flow-through test” method (more adapted to sensors for hydrogen quality assessment) and the “chamber test” method (more adapted to fugitive/emission measurement).

In the flow-through testing method (Figure 1 A), the interface of the sensors to the gas line is hermetically sealed to assure that the sensors are subjected to the proper gas composition without any leaks. Several sensors can be tested simultaneously, in parallel or in series (some sensors consume the component they measure) with this method.

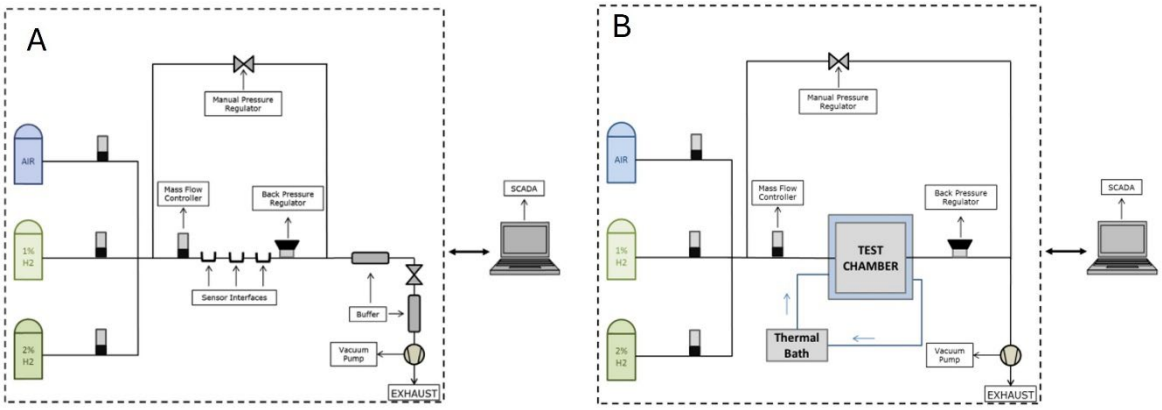

Figure 1: Set-up for a flow-through test (A) and chamber test (B) method according to ISO 26142.

© RISE Research Institutes of Sweden

In the “chamber test” method (Figure 1 B), the sensors are placed in a micro-chamber where flow-through conditions are simulated. The environmental parameters can be easily controlled. The number of sensors that can be tested simultaneously depends upon the size of the chamber.

In this study, we used “flow-through test” method for MPS and NPS sensor and “chamber test” method for the AI prediction sensor.

The rig includes test gases, mass flow controllers, temperature, pressure, and humidity controllers/monitors, control system and safe flow path, including vent and pressure relief. All measurements with gases were performed in well-ventilated areas and under a fume cupboard.

2.2.1 Test gases

The rig has four lines for the supply of gases. All gases used were certified reference material (provided values with traceability links to units of the International System (SI)). Each line is built with chemically inert tubing, pressure rating suitable for the operating conditions and an on-off valve for safety reasons. The four lines are connected using tee-connectors. After the tee-connectors, the gases reach a mixing tube which ensures that the gases are well mixed.

In this study, several gas mixtures were used including a gas containing 4 ± 0.08 vol-% of hydrogen in nitrogen and a gas containing 1 ± 0.02 vol-% of hydrogen in nitrogen. The other gas mixtures were: $N_2/CO/O_2$ at 73.46/7/19.54 vol-% and $N_2/CO_2/O_2/CH_4$ at 68.34/12/18.16/1.5 vol-%. Different gas mixtures concentrations were generated from blending the H_2 reference gases and the other mixtures. The gas changes were done effectively using a mixing device in the rig and the composition of the resulting gas was verified using a gas chromatography with thermal conductivity detector (GC-TCD) as reference analytical instrument.

2.2.2 Mass flow controllers

The four lines for the supply of gases were each equipped with a calibrated Laminar Flow Element (LFE) flow controller (MC Series, Alicat, Tucson, USA), for which the volumetric flow rate is a function of the pressure difference and the viscosity of the gas to be measured. Flow ranges are: 0-5000 mL/min, 0-2000 mL/min, 0-500 mL/min, and 0-100 mL/min. The flow controllers were connected with fast connections so they can easily be moved from one line to the other depending on the gases and the required gas composition.

2.2.3 Temperature controllers

All sensors’ tests were performed at room temperature (~24°C). The temperature was controlled by the rig.

2.2.4 Pressure controllers

The pressure during the test was controlled using the gas cylinders regulators. In addition, it can be read on the flowmeters which can measure mass flow and pressure

© RISE Research Institutes of Sweden

simultaneously. In this configuration, the rig allows only to test sensors at atmospheric pressure.

2.2.5 Humidity controllers

The tests were done at 0% RH as the manufacturer indicated that the sensors did not need humidity to function. This was the case for all tests performed in this study.

2.2.6 Control system

The control system used to collect the data was supplied by the sensors suppliers. The data-acquisition interval was 2 s for the MPS sensor, 0.5 s for the NPS sensor, and 10 s 5 times followed by 2 minutes pause for the AI prediction sensor.

2.3 Experimental Procedure

For sensor evaluation tests two gas compositions were chosen. First one was called "LSOC" and the second one was called "HSOC". These gases were then diluted with air so $H_2/CO_2/CO/CH_4$ ratio close to 1/8.5/0.5/1 for LSOC and 1/0.7/1.7/0.1 for HSOC were kept during all test series.

2.3.1 MPS sensor technology

The composition of the gas mixtures used is presented in Table 1.

Measurements started with clean air and H_2 at 1 vol-% to reach initial stability. After that, consecutive tests/cycles of approximately 240 s (4 min) each with 180 s (3 min) exposure to clean air in between each test (reach stability on each step) were performed. After the final cycle, H_2 in air was assessed to evaluate the sensor recovery after exposure to the gas mixtures.

Each measurement was performed as replicate. In addition, samples from the gas mixtures were taken to confirm gas composition with GC-TCD.

The sensor response was % LEL. Response time and bias was calculated in each case. T90 and T10 was evaluated as the average of the replicates. Bias and relative bias was calculated by the following equations:

$$b = \bar{x} - x_{ref} \qquad \text{(Eq. 1)}$$

$$b(\%) = \frac{\bar{x} - x_{ref}}{x_{ref}} \times 100 \quad \text{(Eq. 2)}$$

Where b is bias, $\bar{x}$ is the average of measured LEL concentration, x_{ref} is the theoretical LEL concentration and b(%) is relative bias.

© RISE Research Institutes of Sweden

Table 1: Gas mixture composition for “LSOC” and “HSOC” during MPS sensor testing.

Gas mixtures	H_2 vol%	O_2 vol%	N_2 vol%	CO vol%	CO_2 vol%	CH_4 vol%
Test series 1: Low SOC						
1	1.00	14	76	0.47	8.2	1.03
2	0.8	15	76	0.42	7.0	0.87
3	0.63	16	76	0.29	5.7	0.71
4	0.43	18	77	0.20	4.0	0.50
5	0.26	19	78	0.13	2.7	0.34
6	0.13	20	78	0.07	1.3	0.17
7	0.08	20	78	0.05	1.0	0.12
Test series 2: High SOC						
1	0.77	4.32	92.65	1.29	0.52	0.07
2	0.65	6.91	90.54	1.08	0.44	0.05
3	0.53	9.62	88.30	0.90	0.35	0.04
4	0.40	12.36	86.07	0.67	0.27	0.03
5	0.30	14.61	84.21	0.51	0.21	0.03
6	0.19	16.81	82.42	0.33	0.13	0.02

2.3.2 NPS sensor technology

Tests were performed using “flow-through test” method. Test series 1 (LSOC) and Test series 2 (HSOC) included the gas mixture containing the maximum and minimum concentration of H_2 (Table 2).

LSOC measurements started with 20 min in clean air followed by exposure to H_2 at 4 vol-% to reach initial stability. After that, three different cycles were tested, first one with H_2 (1%) and second and third one at the highest and respective lowest gas mixture concentration (Table 2). Test/cycles of approximately 10 min each followed by 5 min exposure to clean air in between each test (reach stability on each step) were performed. After the final cycle, the sensor was exposed to clean air during around 1 h and a final test was done using H_2 (1 vol-%) to evaluate sensor recovery after gas mixture exposure. Gas mixture 1 was tested again after H_2 (1 vol-%) and the sensor recovery.

For the HSOC tests, the tests were performed on two different days. Both started with 20 min in clean air and then exposure to H_2 at 1 vol-% to reach stability. After that, a gas mixture with the lowest concentration (H_2 0.19 vol-%) was tested (on day 1), while the gas mixture with the highest concentration (H_2 0.77 vol-%) was assessed on day 2.

© RISE Research Institutes of Sweden

Cycles of approximately 5 min each followed by 3 min exposure to clean air in between each test (reach stability on each step) were performed. After the final cycle (both on day 1 and 2), the sensor was exposed to clean air and a final test was done with H_2 in air (0.18 vol-% and 1 vol-%) on day 1 and H_2 at 0.77 vol-% on day 2, to evaluate sensor recovery after gas mixture exposure.

Each measurement was performed as replicate. In addition, samples of the gas mixtures were taken to confirm the gas composition using a GC-TCD analysis. Response time and bias were calculated as previous stated in 2.3.1. The sensor response was expressed as H_2 vol-%.

Table 2: Gas mixture composition for low SOC and high SOC in NPS sensor.

Gas mixtures	H_2 vol%	O_2 vol%	N_2 vol%	CO vol%	CO_2 vol%	CH_4 vol%
Test series 1: Low SOC						
1	0.97	14	75	0.46	8.3	1.04
2	0.18	20	78	0.09	1.6	0.20
Test series 2: High SOC						
1	0.77	4	93	1.32	0.53	0.07
2	0.19	17	82	0.37	0.13	0.02

2.3.3 AI prediction sensor technology

Tests were performed using “chamber test” method. Test series 1 (LSOC) and Test series 2 (HSOC) started from H_2 0.97 vol-% and 0.77 vol-%, respectively followed by dilution with air until H_2 was around 0.1 vol-% (Table 3) (the ratio of gases remained stable). Measurement started with 15 min in clean air. After that, cycles with the different gas mixtures were tested. Test/cycles of approximately 5 min each followed by 3 min exposure to clean air in between each test (to reach stability on each for these experiences with 5 measurements with 10 s apart and after that 2 min without measurement controlled by the sensor provider´s software). The sensor signal was qualitative i.e. detected/non-detected response.

Samples from the gas mixtures were taken to confirm gas composition with GC-TCD.

© RISE Research Institutes of Sweden

Table 3: Gas mixture composition for LSOC and HSOC in AI Prediction sensor.

Gas mixtures	H_2 vol%	O_2 vol%	N_2 vol%	CO vol%	CO_2 vol%	CH_4 vol%
Test series 1: Low SOC						
1	0.97	14	75	0.46	8.3	1.04
2	0.81	15	76	0.38	6.9	0.87
3	0.65	16	77	0.31	5.6	0.69
4	0.47	18	77	0.22	4.0	0.50
5	0.33	19	78	0.15	2.8	0.35
6	0.18	20	78	0.09	1.6	0.20
7	0.14	20	78	0.07	1.2	0.15
Test series 2: High SOC						
1	0.77	4	93	1.32	0.53	0.07
2	0.65	7	90	1.11	0.45	0.06
3	0.52	10	88	1.03	0.36	0.05
4	0.40	12	86	0.78	0.27	0.03
5	0.29	15	84	0.57	0.20	0.03
6	0.19	17	82	0.37	0.13	0.02
7	0.13	18	80	0.23	0.12	0.01

© RISE Research Institutes of Sweden

3 Results

3.1 MPS sensor evaluation

3.1.1 Test series 1: LSOC

Figure 2 shows the %LEL for the different gas mixtures when tested LSOC mixtures.

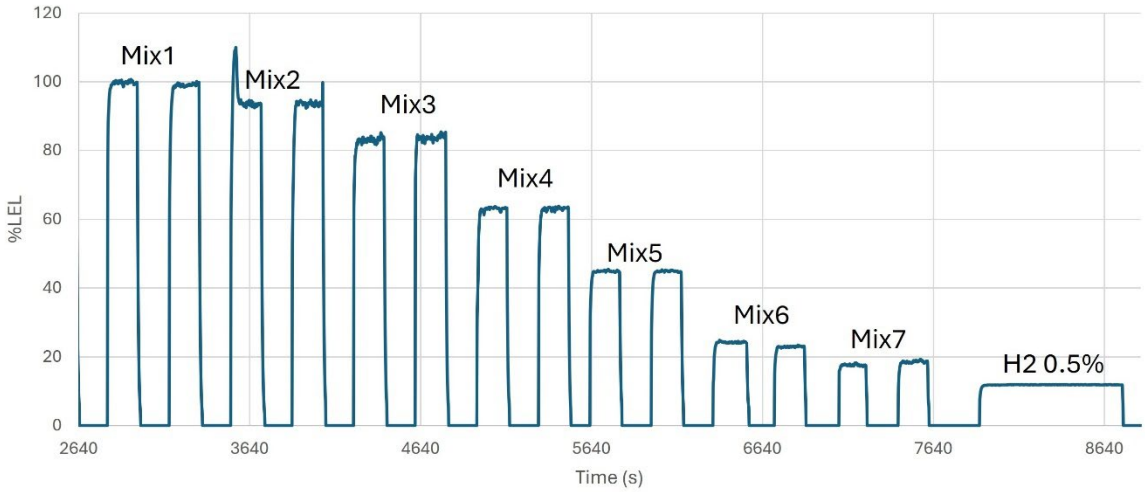

Figure 2: Percentage of LEL for all the gas mixtures tested.

As expected, a decrease in %LEL is observed when flammable gas concentration decreased in the gas mixtures. However, the measured %LEL in mixtures is higher than the expected theoretical values as can show in Figure 3.

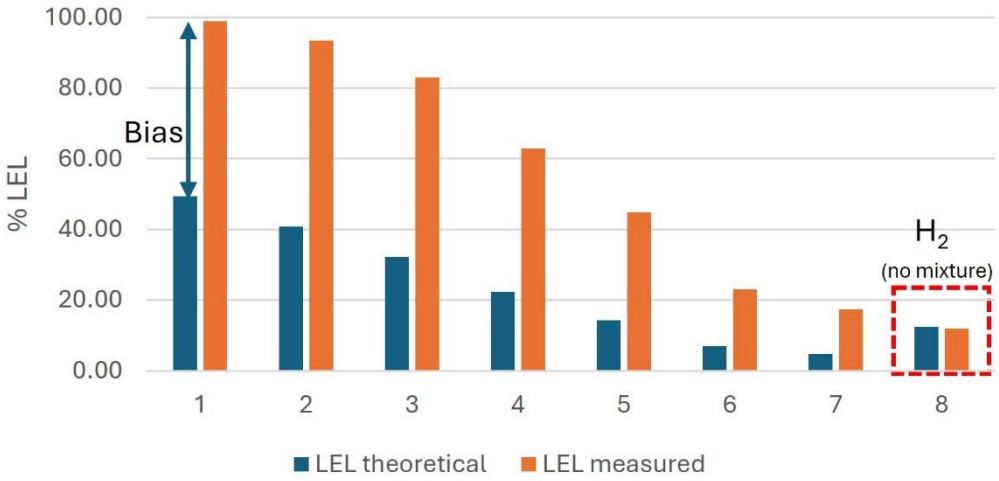

Figure 3: Comparison between %LEL theoretical and measured %LEL with MPS sensor for LSOC.

© RISE Research Institutes of Sweden

Figure 3 shows that %LEL was overestimated in all the gas mixtures, which is linked to CO_2, being detected as a flammable gas. To demonstrate this effect, the sensor was exposed to only H_2 and the result showed this time a good agreement between the theoretical and measured %LEL.

Table 4 shows the obtained values for %LEL theoretical and measured, as well as bias for the three last measurements. The relative bias is stable at around 200%. The response time T90 was estimated to be 11-16 seconds and the recovery time 6 to 8 seconds.

Table 4: Bias, relative bias and response time for the gas mixtures in LSOC.

Parameters/Gas mixtures	Mix 5	Mix 6	Mix 7
% LEL theorical	15,29	9,17	6,87
% LEL measured	46,00	27,00	20,50
Bias	30,71	17,83	13,63
Relative bias (%)	200,93	194,42	198,25
Recovery time (T10)	6-8 s		
Response time (T90)	11-16 s		
Ratio			
CO	0.47	0.48	0.46
CO_2	8.39	8.56	9.06
CH_4	1.05	1.07	1.13

As can be shown in Table 5, there was a good agreement between the gas composition calculated using the flow rates and the gas composition measured using a GC-TCD ensuring therefore, the well-functioning of the rig.

Table 5: Gases composition calculated through flowmeter (rig) and GC-TCD

Gas mixtures	Concentration calculated by	H_2 vol%	O_2 vol%	N_2 vol%	CO vol%	CO_2 vol%	CH_4 vol%
1	Flowmeter (rig)	1	13.79	75.58	0.47	8.21	1.03
	GC-TCD	1	13.25	75.79	0.46	8.29	1.02
7	Flowmeter (rig)	0.08	20.35	78.43	0.05	0.98	0.12
	GC-TCD	0.07	20.45	78.38	0.05	0.95	0.11

© RISE Research Institutes of Sweden

3.1.2 Test series 2: HSOC

Figure 4 shows the %LEL for the different gas mixtures when tested HSOC.

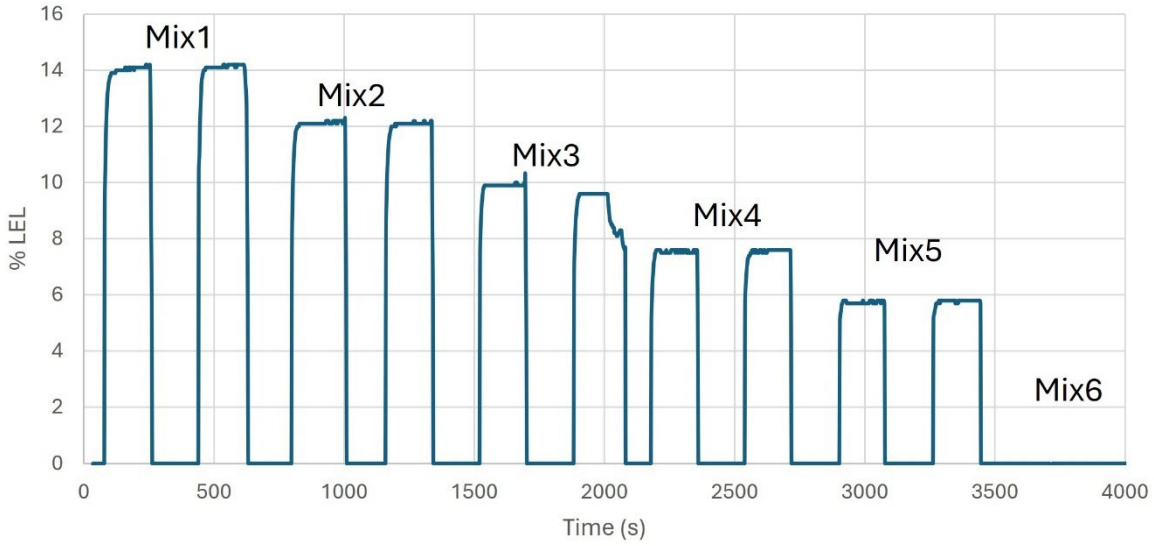

Figure 4: Percentage of LEL for all the gas mixtures tested.

As H_2 concentration decreases in the gas mixture, % LEL decrease too. However, for gas mixture 6 corresponding to the lowest mixture gas composition, no sensor response was observed.

Figure 5 shows that %LEL was underestimated in all the gas mixtures compared to the theoretical values, which can be due to the fact that CO, which is a flammable gas, was not detected by the sensor as it can be seen in the test where the sensor was only exposed to CO (no response).

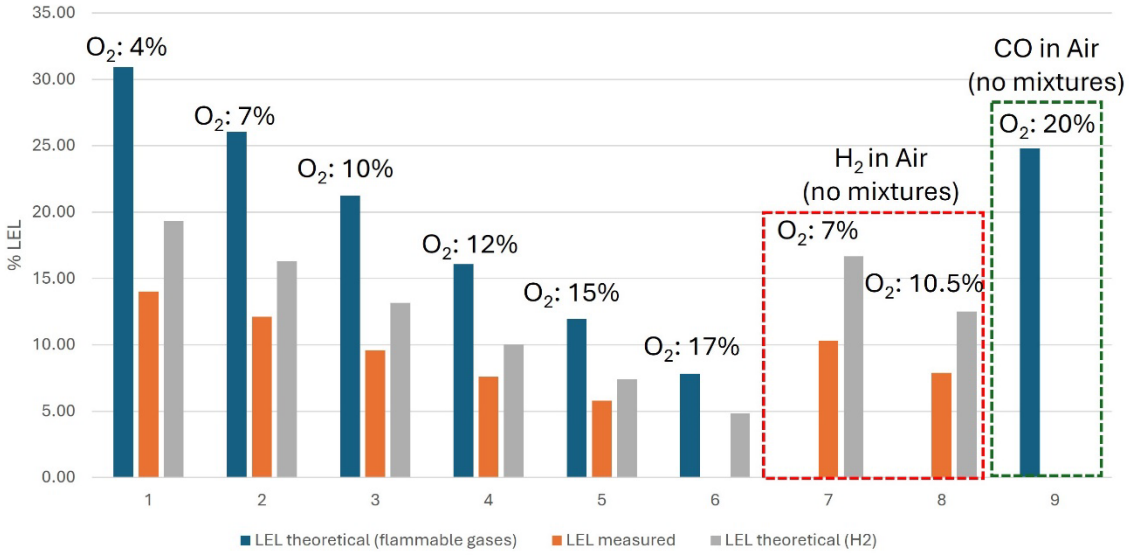

Figure 5: Comparison between LEL theoretical and measured LEL with MPS sensor for HSOC.

© RISE Research Institutes of Sweden

As can be observed in Figure 5, the expected %LELs, taking into account all the flammable gases (blue bars) in the gas mixture, are higher than the measured %LELs (orange bars). However, when theoretical %LEL is calculated taking into account only H_2 as flammable gas (grey bars) in the gas mixture, these values are more similar to the measured LEL. Therefore, it seems that the sensor only "sees" H_2 as flammable gas while the other gases are not detected.

Table 6 shows the obtained values for %LEL theoretical and measured, as well as bias for the four last measurements. The relative bias is around -50% for mixtures 3, 4 and 5 but much higher for mixture 6 (-100%).

The response time T90 for the sensor in this test series was estimated to be 8 to 10 seconds and the recovery time T10 was estimated to be 2 to 4 seconds.

Table 6: Bias, relative bias and response time for the gas mixtures in HSOC.

Parameters/Gas mixtures	Mix 3	Mix 4	Mix 5	Mix 6
% LEL theoretical[a]	21.21	16.06	11.96	7.83
% LEL theoretical (H_2)[b]	13.16	10.00	7.39	4.85
% LEL measured	9.60	7.60	5.80	0.00
Bias[c]	-11.61	-8.46	-6.16	-7.83
Relative bias (%)[c]	-55	-53	-51.5	-100
Recovery time (T10)	2-4 s			
Response time (T90)	8-10s			
Ratio				
CO	1.70	1.69	1.71	1.71
CO_2	0.66	0.66	0.70	0.66
CH_4	0.08	0.08	0.09	0.08

[a] considering all flammable gases

[b] considering only H_2 as flammable gas

[c] calculated assuming LEL theoretical for all flammable gases.

As can be shown in Table 7, the gases concentration for mixture 5 calculated using the flow rates set in the rig and with a GC-TCD analysis were in good agreement, confirming therefore, the well-functioning of the rig.

Table 7: Gases composition calculated through flowmeter (rig) and GC-TCD

Gas mixtures	Concentration calculated by	H_2 vol%	O_2 vol%	N_2 vol%	CO vol%	CO_2 vol%	CH_4 vol%
5	Flowmeter (rig)	0.30	14.61	84.21	0.51	0.21	0.03
	GC-TCD	0.33	14.58	84.42	0.47	0.19	0.02

© RISE Research Institutes of Sweden

3.1.3 Signal stability

Figure 6 shows the stability of the signal when the sensor was exposed to the gas mixtures series and when the sensor was exposed only to H_2. It can be seen that the signal was stable when the sensor was exposed to gas mixture "HSOC" and to H_2, but not when the sensor was exposed to the gas mixture "LSOC".

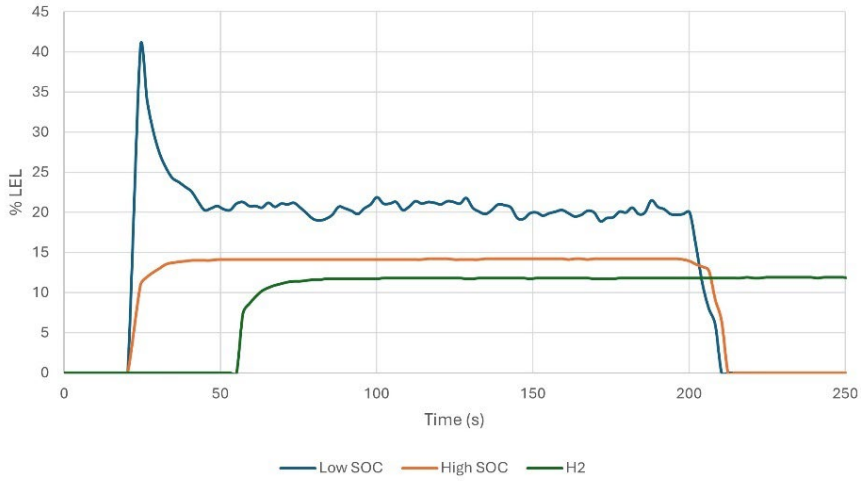

Figure 6: Signal stability for LSOC, HSOC and H_2.

3.2 NPS sensor evaluation

3.2.1 Test series1: LSOC

The tests performed on a first sensor showed lower T90 than expected by the sensor provider/developer and some problem with the kinetics. A new sensor was then provided by the sensor developer, and all tests were performed on this sensor. The first tests focus on T90 for only hydrogen in air to confirm the sensor was responding as expected by the sensor provider/developer (Figure 7).

Figure 7 also shows the H_2 vol-% measured when the sensor was exposed to the gas mixtures. When exposed to H_2 4 and 1 vol-% respectively (without any other gases), the sensor response was in good agreement with the theoretical value. However, as soon as the sensor was exposed to any gas mixtures, the response was underestimated.

© RISE Research Institutes of Sweden

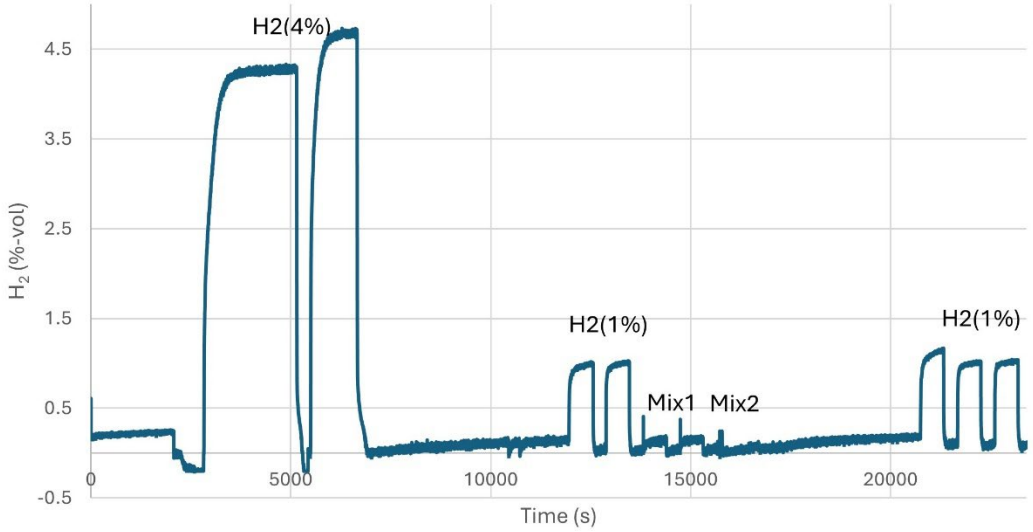

Figure 7: Percentage of H_2 for the gas mixtures tested in LSOC test series.

Figure 8 shows clearly the influence of the other gases on the sensor response, which demonstrates that other gases act as interferences and inhibit the response of the sensor. For example, for gas mixture 1 where $H_2/CO/CO_2/CH_4$ concentration is 0.97/0.46/8.3/1.04 vol-%, the response of the sensor is much lower than expected (around 0.1 vol-% instead of 0.97). For the mixture 2 where $H_2/CO/CO_2/CH_4$ is 0.18/0.09/1.6/0.20 vol-%, the response is 0.02 instead of 0.18.

However, the sensor recovers well as it can be seen in test 6 (the sensor is then only exposed to H_2 after all the tests with the gas mixtures) where the response is similar to test 1 (test performed before the sensor is exposed to any gas mixture).

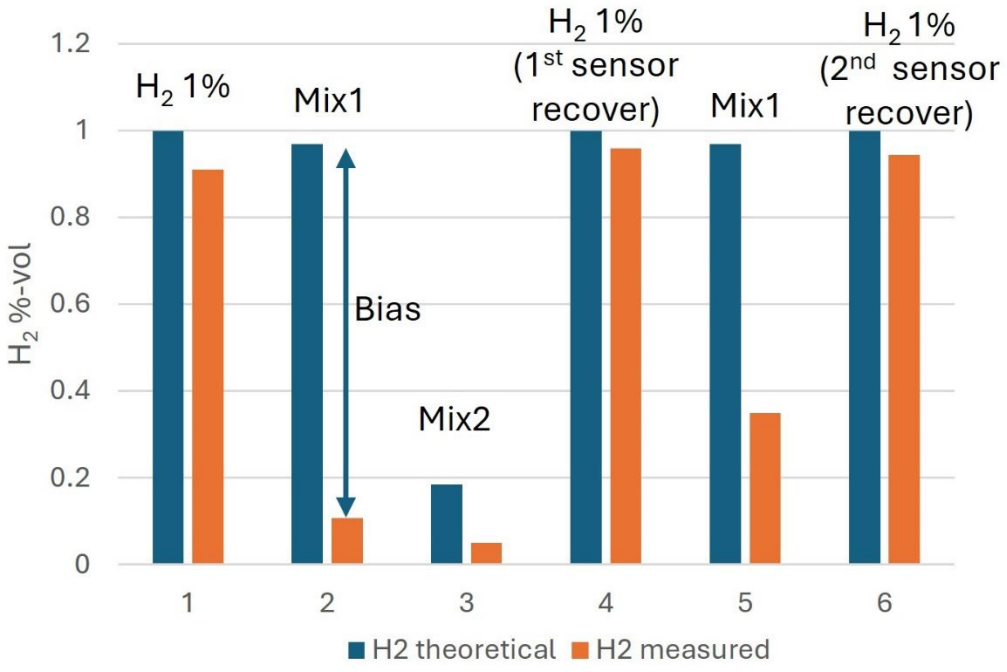

Figure 8: Comparison between H2 %-vol theoretical and measured for NPS sensor.

© RISE Research Institutes of Sweden

Table 8: Bias, relative bias and response time for the gas mixtures in LSOC and sensor recovery tests.

Parameters/Gas mixtures	H_2(1 vol-%)	Mix 1	H_2 (1 vol-%)[a]	H_2 (1 vol-%)[b]
% H_2 theoretical	1	0.90	1	1
% H_2 measured	0.91	0.11	0.96	0.94
Bias	-0.09	-0.79	-0.04	-0.09
Relative bias (%)	-9	-88	-4	-9
Recovery time (T10)	2 s	24.2 s	1-2 s	2 s
Response time (T90)	14 s	156s	13 s	13 s

[a] 1st sensor recovery (H_2 in air)
[b] 2nd sensor recovery (H_2 in air)

Table 8 shows the values measured H_2 vol-% as well as the theoretical H_2 vol-%, together with bias and sensor recovery tests.

For the gas mixture, the response of the sensor is greatly underestimated (bias -88%). The response time T90 when the sensor is exposed only to H_2 is around 13-14 seconds while the T90 when the sensor is exposed to the gas mixture is much longer (156 seconds). The T10 when the sensor is exposed to only H_2 is very short (1-2 seconds) while the T10 when the sensor is exposed to the gas mixture is much longer (24 seconds).

As can be shown in Table 9 the gases concentration in mixture 2 calculated using the flowrates given by the rig and GC-TCD analysis were similar, confirming therefore, the well-functioning of the rig.

Table 9: Gases composition calculated through flowmeter (rig) and GC-TCD

Gas mixtures	Concentration calculated by	H_2 vol%	O_2 vol%	N_2 vol%	CO vol%	CO_2 vol%	CH_4 vol%
2	Flowmeter (rig)	0.184	19.56	77.60	0.09	1.62	0.20
	GC-TCD	0.22	19.56	78.40	0.08	1.56	0.18

3.2.2 Test series 2: HSOC

Figure 9 shows the H_2 vol-% measured by the sensor when exposed to hydrogen and to the gas mixture "HSOC". Once again, the sensor responded as expected when exposed only to hydrogen but much lower than expected when exposed to the gas mixture "HSOC" (tests done with a mixture containing ~0.8 vol-% H_2 (response 0.22 vol-% H_2) and a mixture containing 0.18 vol-% H_2 (response could not be registered), as shown in Figure 10.

© RISE Research Institutes of Sweden

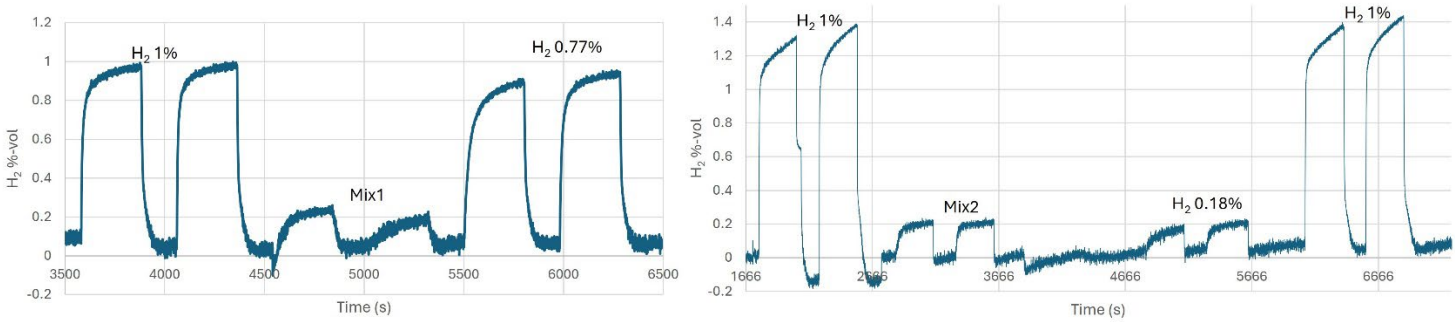

Figure 9: H_2 vol-% for the tested gas mixtures in HSOC.

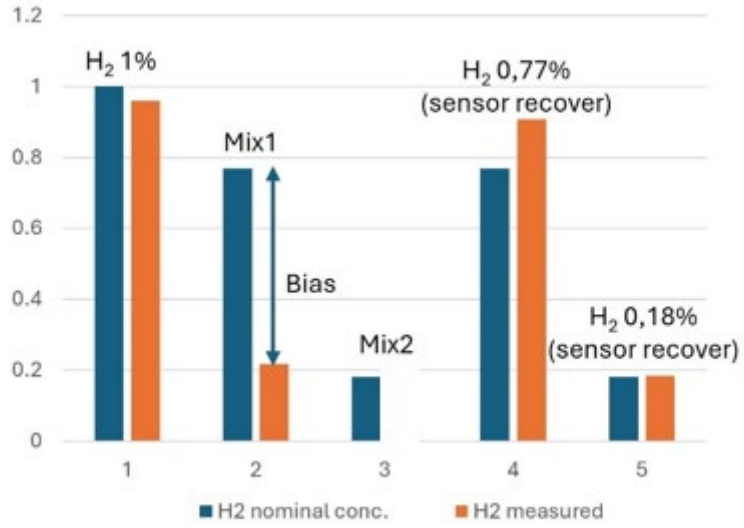

Figure 10: Comparison between H_2 vol-% theoretical and measured for NPS sensor in HSOC test series.

The low H_2 vol-% values registered by the sensor in mixture 1 (Figure 10) shows that the presence of other gases in the gas mixture, particularly CO and CO_2 affect the H_2 response.

However, the sensor recovers well when exposed to hydrogen at the end of the test series.

© RISE Research Institutes of Sweden

Table10: Bias, relative bias and response time for the gas mixtures in HSOC and sensor recovery tests.

Parameters/Gas mixtures	H_2(1 vol-%)	Mix 1	Mix 2	H_2 (0.77 vol-%)[a]
% H_2 theoretical	1	0.77	0.19	0.77
% H_2 measured	0.96	0.21	-	0.91
Bias	-0.04	-0.56	-0.19	0.14
Relative bias (%)	-4.01	-72.60	-100	18
Recovery time (T10)	13 s	22 s	12 s	10 s
Response time (T90)	53 s	233 s	128 s	95 s

[a] sensor recovery H_2 in air at 0.77%-vol.

The response time T90 is higher when the sensor is exposed to the gas mixtures than when the sensor is only exposed to hydrogen, however this time, the response time seems to be negatively influenced by the interferences as the response time done at the end of the test series when the sensor is only exposed to hydrogen again (95 seconds) is longer than in the beginning of the test series (before the sensor was exposed to any gas mixtures), as shown in Table 10.

3.2.3 Signal stability

As it can be seen in Figure 11 and 12, the signal was quite unstable and kept on increasing. Therefore, T90 was calculated using an average for the response.

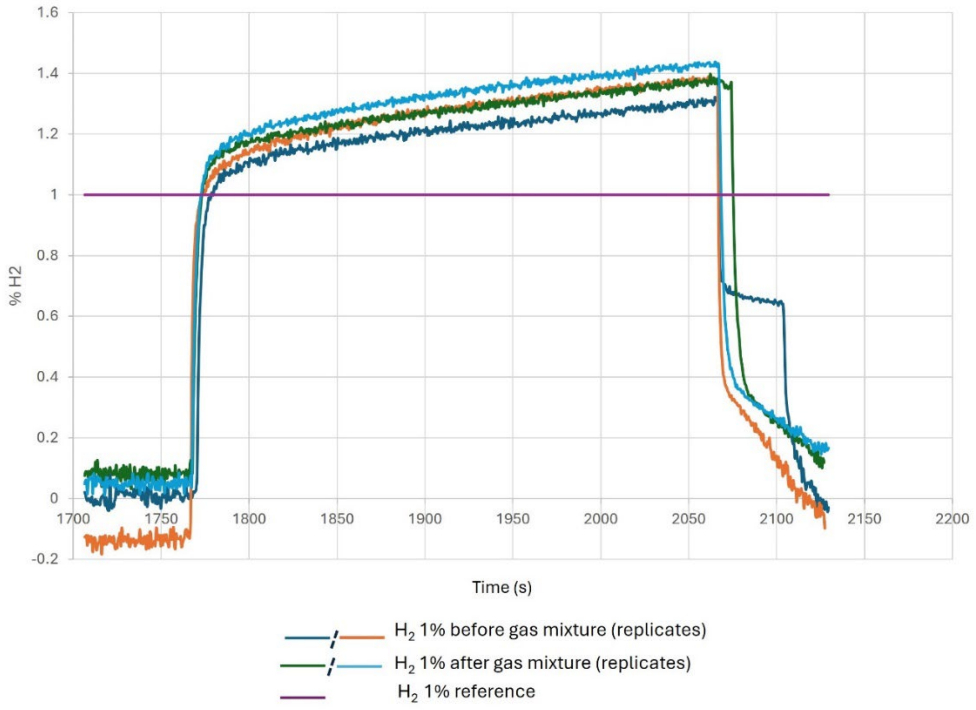

Figure 11: H_2 1 vol-% in air before and after gas mixtures.

© RISE Research Institutes of Sweden

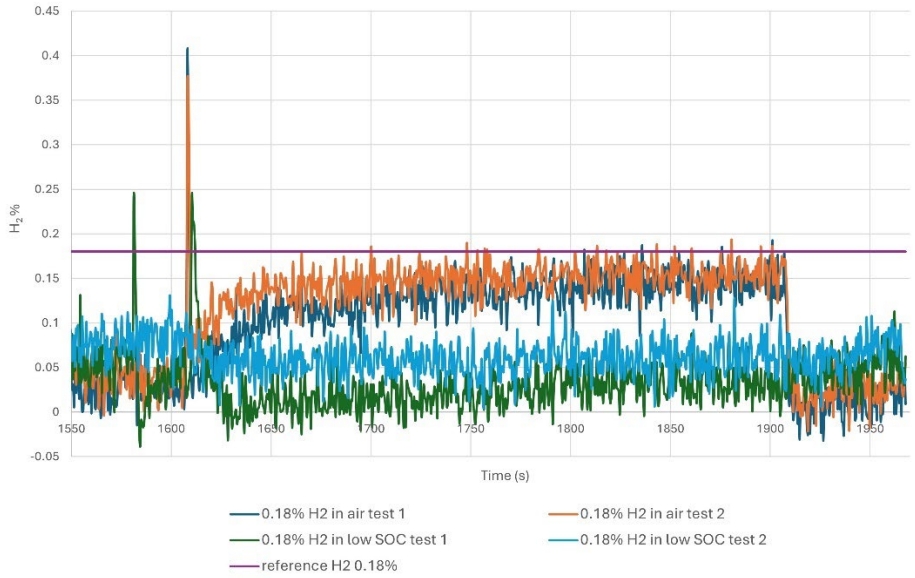

Figure 12: H_2 vol-% response for LSOC test in gas mixture 2 (H_2 0.18 vol-%) and H_2 0.18 vol-% in air.

The sensor was tested again by the sensor´s provider and the performance returned to normal levels, which indicates that the sensor chips recovers after exposure to CO.

3.3 AI prediction sensor evaluation

3.3.1 Test series: LSOC and HSOC

The sensor was first trained for specific gases using both mixtures HSOC and LSOC and dilution of these mixtures in air. Figure 13 shows that the sensor reacted to all the gas mixtures it was exposed to, the response being “detected” without indication of concentrations.

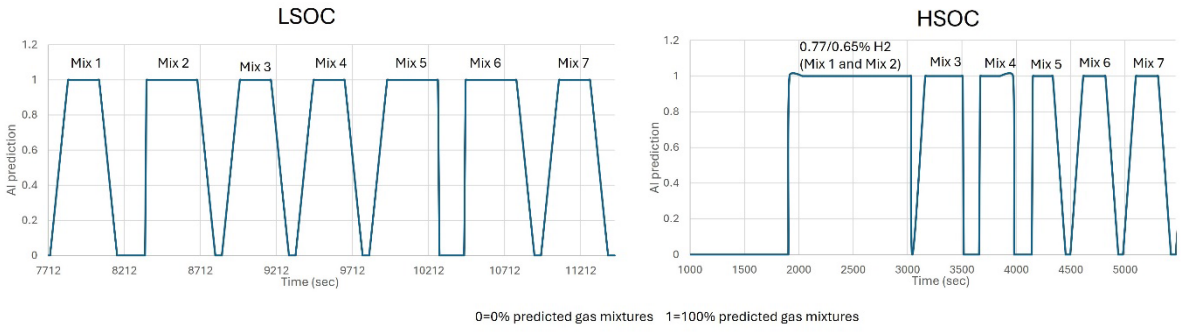

Figure 13: AI-prediction for the gas mixtures in LSOC and HSOC test series.

For this sensor, as no quantitative data can be obtained, bias cannot be calculated. T90 and T10 could not be calculated neither as the sensor registered a signal every 10 seconds followed by 2 minutes pause.

© RISE Research Institutes of Sweden

Table 11 shows the gases composition in mixture 1 for both HSOC and LSOC test series calculated using the flowrates on the rig and the results from the GC-TCD analysis. Results were in good agreement, confirming therefore, the well-functioning of the rig.

Table 11: Gases composition calculated through flowmeter (rig) and GC-TCD

Gas mixtures	Concentration calculated by	H_2 vol%	O_2 vol%	N_2 vol%	CO vol%	CO_2 vol%	CH_4 vol%
HSOC/ Mixture 1	Flowmeter (rig)	0.77	4.41	92.94	1.30	0.52	0.06
	GC-TCD	0.74	4.46	92.12	1.32	0.52	0.07
LSOC/ Mixture 1	Flowmeter (rig)	0.98	13.79	75.46	0.46	8.26	1.03
	GC-TCD	0.99	13.20	75.56	0.49	8.15	1.07

4 Conclusions

The performance of MPS, NPS, and AI-prediction sensors was evaluated with gas mixtures containing H_2, CO, CO_2, CH_4 at defined ratios ($H_2/CO_2/CO/CH_4$ ratio close to 1/8.5/0.5/1 and 1/0.7/1.7/0.1 respectively).

MPS sensor showed fast response times (11-16 s for T90) and stable signals, but exhibited measurement bias due to interferences. In LSOC, %LEL values were overestimated, due to CO_2 being considered by the sensor as a flammable gas, while in HSOC they were underestimated, as it seems that CO which is a flammable gas was not detected.

NPS sensor accurately measured H_2 in air but underestimated hydrogen concentrations in the tested gas mixtures, confirming cross-sensitivity to CO and CO_2. However, the response of sensor recovered well. Another issue was that the signal was often unstable (kept on increasing) and noisy during some measurements even when exposed to only hydrogen. In addition, this sensor requires some conditioning in air and H_2 before measurement's cycles.

AI-prediction sensor qualitatively detected all gas mixtures under both LSOC and HSOC, regardless of concentration, which potentially could be useful for early gas detection applications. However, trueness and response time could not be calculated in this study, and to evaluate the sensor performance those are important parameters. It would be important to improve the data acquisition system.

The obtained results emphasize that gas mixture composition strongly affects sensor response. MPS and NPS sensors were particularly sensitive to interferences/gases normally present when lithium-ion batteries undergo TR.

© RISE Research Institutes of Sweden

Appendix 3: Battery electric vehicle tests

Authors: Ola Willstrand, Anna Karlsson

1 Introduction

The battery electric vehicle (BEV) tests were conducted in collaboration with the Carbon diOxide Fire Fighting Experimental Evaluation (COFFEE) project, funded by the Swedish Mercantile Marine Foundation and the Swedish Transport Administration and coordinated by RISE Research Institutes of Sweden. The COFFEE project was the main financial contributor for the tests and made all the decisions regarding test setup and test procedure. In the COFFEE project, the objective of the tests was to evaluate how effectively a total-flooding carbon dioxide system can suppress fire in both internal combustion engine vehicle (ICEV) and BEV under conditions representative of a vehicle carrier ship. The experiments specifically assessed the performance of CO_2 to suppress vehicle fire by preventing battery TR propagation, limiting fire spread to other parts of the vehicle and preventing spread to adjacent vehicles in an enclosed cargo space of a ship.

The objective of the EDOT project in these tests was to evaluate detectors' response time in relation to the placement of different type of sensors in a large-scale test environment with a BEV. A few of the best performing sensors from the cell-level tests [*separate article, reference will be added when published*] were installed. As the CO_2 system was not activated until the fire reached approximately 2 MW, response time evaluation tests could be performed during the early stage of the tests. Furthermore, evaluating the possibility of extracting information from the sensors during an event was possible also after the activation of CO_2. This is considered essential by firefighters when managing battery fire incidents.

Details on the test methodology and results relating to the CO_2 suppression tests are presented in the test report from the COFFEE project [*reference will be added when that report is published*]. Here, a brief summary of the general test methodology is given followed by details regarding the installation of gas and smoke sensors, as well as results and conclusions relating to the response of these detectors.

2 Methodology

Three vehicle fire suppression tests were performed, one involving an ICEV and two involving BEVs. This allowed for assessment of the ability of CO_2 flooding to suppress different types of vehicle fires. However, the detectors evaluated in the EDOT project were only included in the two BEV tests, why these two tests are the ones described in this report.

© RISE Research Institutes of Sweden

2.1 Test setup

The experiments were performed under a large-scale calorimeter hood, allowing determination of fire size during the early stage of the tests when the test compartment was open. To simulate a closed vehicle deck compartment, a dedicated fire test enclosure was constructed inside the fire test hall. The compartment had internal dimensions of approximately 6.7 m × 3.1 m × 3.0 m (length × width × height), corresponding to an internal volume of about 62 m³. Although substantially smaller than a full-scale vehicle deck, the chosen dimensions represented a repeatable, practical and economically feasible test configuration within the scope of the project. The compartment was equipped with a removable roof consisting of two large hatches that remained open during the initial free-burn phase and were closed immediately before CO_2 discharge, see Figure 1. The roof hatches also incorporated numerous small pressure-relief panels designed to accommodate pressure increases during CO_2 flooding and potential explosion events. The vehicles were positioned on a purpose-built weighing platform mounted on load cells.

Figure 1. Photo inside the fire test enclosure showing the roof with large hatches that were open during the free-burn phase and closed immediately before CO_2 discharge.

2.1.1 Test vehicles and fire initiation

Two representative modern passenger BEVs were selected for testing, one with lithium iron phosphate (LFP) pouch cells (BEV1), and one with lithium nickel manganese cobalt oxide (NMC) prismatic cells (BEV2). Prior to testing, components such as airbags and pressurized devices were removed or rendered safe. Battery SOC levels were deliberately increased to approximately 90% to maximize the likelihood of TR propagation, despite that realistic SOC levels during vehicle transport at sea are typically below 50%. TR was induced by mechanical penetration of a battery module using a pneumatically driven steel nail. A secondary ignition method, employing an oxy-acetylene cutting torch, was prepared if the nail penetration would fail to initiate

© RISE Research Institutes of Sweden

TR. In practice, BEV1 required the cutting torch to initiate TR, whereas BEV2 successfully entered TR through nail penetration.

2.1.2 Carbon dioxide suppression system

The suppression system consisted of several 50-litre cylinders containing nominally 37.5 kg of CO_2 each. The cylinders were connected through a common manifold and supplied via two discharge nozzles mounted on the inside wall of the test compartment. Three cylinders were discharged simultaneously at the start of each suppression test. Calculations show that this quantity would generate approximately 45 vol-% CO_2 within the enclosure, equivalent to an oxygen concentration of about 11.5 vol-%, consistent with the design concentration required for shipboard CO_2 systems protecting vehicle spaces[1]. Additional cylinders were activated individually during the monitoring period to compensate for leakage and maintain low (11.5 vol-%) oxygen concentrations.

2.1.3 Gas and smoke sensors

Four different types of sensors were installed in the tests, all of which performed well in the cell-level tests. They are listed in Table 1 with a short description of the technology, detectable gases, and alarm thresholds, if provided by the supplier. The Li-ion Tamer detector has a patented technology and alarm algorithm specifically designed for early detection of battery off-gassing events with a specific focus on detection of LIB electrolyte vapours. The EC H_2 and EC CO are standard industry gas detectors used e.g. in the marine and energy sectors, and the industrial fire detector has both a smoke sensor and a heat sensor (individual alarm signals).

Table 1. Evaluated sensors

Name	Sensor technology	Detectable gases/signatures	Alarm threshold
Li-ion Tamer	Metal oxide semiconductor	Electrolyte vapour, H_2, CO	
EC H_2	Electrochemical	H_2	100 ppm
EC CO	Electrochemical	CO	50 ppm
Industrial fire detector	Light scattering & thermistor	Smoke and heat	

The four different types of sensors were grouped together at four positions in the test compartment; (A) on the floor adjacent to the vehicle, (B) inside the vehicle cabin, (C) on the test compartment wall at 2 m height from the floor, and (D) on a ceiling beam centred above the vehicle. The sensor locations are illustrated in Figure 2. Note that the roof hatches were open during the initial phase of the tests, however, the sensors at location D were mounted on a fixed ceiling beam rather than on the roof hatches.

[1] Chapter 5, “Fixed gas fire extinguishing” of the International Code for Fire Safety Systems (the FSS Code), paragraph 2.2.1.2

© RISE Research Institutes of Sweden

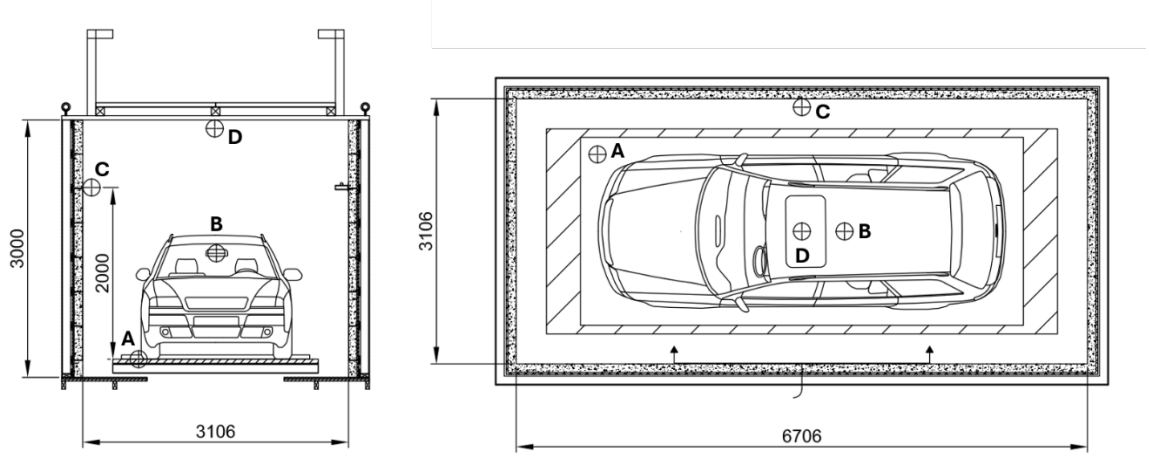

Figure 2. Position of the sensors in the test compartment; A – on the floor, B – inside the vehicle cabin, C – on the wall, and D – in the ceiling.

2.2 Experimental procedure

Each test followed a predetermined sequence. Initially, the roof hatches were fully opened and the fire was initiated. The fire was then allowed to develop under natural ventilation conditions until a total heat release rate of about 2 MW was achieved. At that point, the roof hatches were rapidly closed and immediately after compartment closure, the three CO_2 cylinders were discharged into the test compartment. During a subsequent monitoring period of at least 120 minutes, oxygen concentrations, temperatures, load cell weight measurements, and visual observations were continuously recorded. Whenever oxygen concentrations approached the design threshold, an additional cylinder was discharged to maintain suppression conditions. After the monitoring period, the roof was removed and the compartment was vented. The vehicle was then observed for approximately 60 additional minutes to detect any signs of reignition.

3 Results

Results relating to the CO_2 suppression as well as gas, temperature, and mass loss measurements are presented in the test report from the COFFEE project. Below, a summary of the general test observations is provided, as well as details on the response of the tested sensors.

3.1 General observations

For BEV1, attempts to initiate TR by nail penetration were unsuccessful. In the first attempt the whole vehicle was lifted by the nail rig. In succeeding attempts, the vehicle was strapped down, and the nail was visually penetrating the battery pack. A battery isolation warning was seen in the driver display, but no other signs of battery failure. Therefore, the oxy-acetylene cutting torch was subsequently applied to the underside of the battery pack. Light smoke appeared within seconds, followed by localized flames and intermittent battery venting. A small fire developed underneath the vehicle and gradually spread to adjacent combustible components, towards the left rear

© RISE Research Institutes of Sweden

wheelhouse. As the event progressed, increasing quantities of molten burning material accumulated beneath the vehicle, contributing to flame spread around the rear of the vehicle. By approximately 8 min after ignition, the entire rear section was engulfed in flames. Shortly thereafter, the roof hatches were closed, and the carbon dioxide system was activated. All externally visible flames were extinguished within roughly 20 s of CO_2 discharge, after which smoke obscured further visual observations.

Post-test examination of BEV1 provided valuable information regarding battery involvement. The battery pack exhibited localized external damage at the cutting torch application point and at the opening created for the nail penetration attempt. Disassembly and inspection of the interior of the battery pack revealed extensive damage to nearly all cells in the rear half of the battery pack. In contrast, the front half remained largely intact with retained system voltage. Exterior fire damage was concentrated at the rear of the vehicle, while the passenger compartment experienced limited heat damage in the ceiling and upper parts of interior materials.

For BEV2, TR was successfully initiated by nail penetration and developed much more rapidly than in BEV1. Flames and smoke emerged almost immediately, while the vehicle generated battery fault and fire risk warnings in the driver display. Increasing smoke production was observed from the battery pack and spread beneath the vehicle and through the rear wheelhouses. After approximately 2 min, burning droplets, likely originating from molten plastics or metals, began falling and formed a growing pool fire beneath the vehicle. This secondary fire progressively involved both rear wheelhouses, rear tires, and exterior plastic components. At approximately 7 min 40 s, the test compartment was sealed and flooded with CO_2. The discharge rapidly reduced visibility but extinguished all visible flames before observations became obscured. Following the two hours of monitoring after suppression and venting, no indications of reignition were observed. Fire damage was primarily limited to the rear exterior bodywork and portions of the rear tires. For BEV2, there was no post-test disassembly of the battery pack.

3.2 Gas and smoke sensors response

Figure 3 shows the alarm activation times for all sensors in the four different positions; A – on the floor, B – inside the vehicle cabin, C – on the test compartment wall, and D – on the ceiling beam. The same information is presented in Figure 4 together with the sensors' raw signals. The two electrochemical sensors' raw signal are shown as CO and H_2 concentrations (ppm), while the outputs from the two remaining sensors are presented as normalized values between 0 and 1, where 0 corresponds to the signal value at start of the test and 1 to the maximum sensor response recorded during the test.

For BEV1, as seen in Figure 3a, the Li-ion Tamer sensor alarmed in all positions except inside the cabin, about 1 min after ignition of the cutting torch. This was followed by an alarm for all EC CO sensors in these positions as well as the EC H_2 sensor in the ceiling. The EC H_2 sensors located on the floor and on the wall did not alarm until after discharge of the CO_2 suppression system. Following discharge, smoke and gas concentrations increased as seen in Figure 4, as did the temperatures as seen in Figure 3. This was likely caused by gas mixing and enhanced enclosure sealing. Increased concentrations of flammable gases are also due to the extinguishment of

© RISE Research Institutes of Sweden

visible flames after activation of the CO_2 system. The industrial fire detectors alarmed approximately 2 min after the gas detectors, seen in Figure 3a, coinciding with the entry of smoke and gas into the vehicle cabin. Shortly thereafter, all sensors inside the vehicle alarmed. Notably, the vehicle displayed a warning message indicating high battery temperatures and a request to leave the vehicle only about 1 min before gas and smoke entered the vehicle cabin.

For BEV2, as seen in Figure 3b, a warning message indicating fire risk and a request to leave the vehicle appeared only 7 s after nail penetration of the battery pack. Shortly after, the Li-ion Tamer sensors in the ceiling and on the wall alarmed, followed by the EC CO and the industrial fire detector in the ceiling after 1 min. At approximately 1.5 min, all gas sensors on the floor alarmed, coinciding with increased smoke production underneath the vehicle. This is further supported by the data presented in Figure 4e, which show that the CO and H_2 concentrations increased rapidly from zero to about 500 ppm starting at 1.5 min. All EC CO sensors and industrial fire detectors outside the vehicle cabin alarmed before the EC H_2 sensors on the wall and in the ceiling. Inside the vehicle cabin, the detectors alarmed after about 7 min, just before activation of the CO_2 suppression system. However, the Li-ion Tamer raw signal seen in Figure 4f indicates that gases were present in the cabin as early as 1 min after ignition.

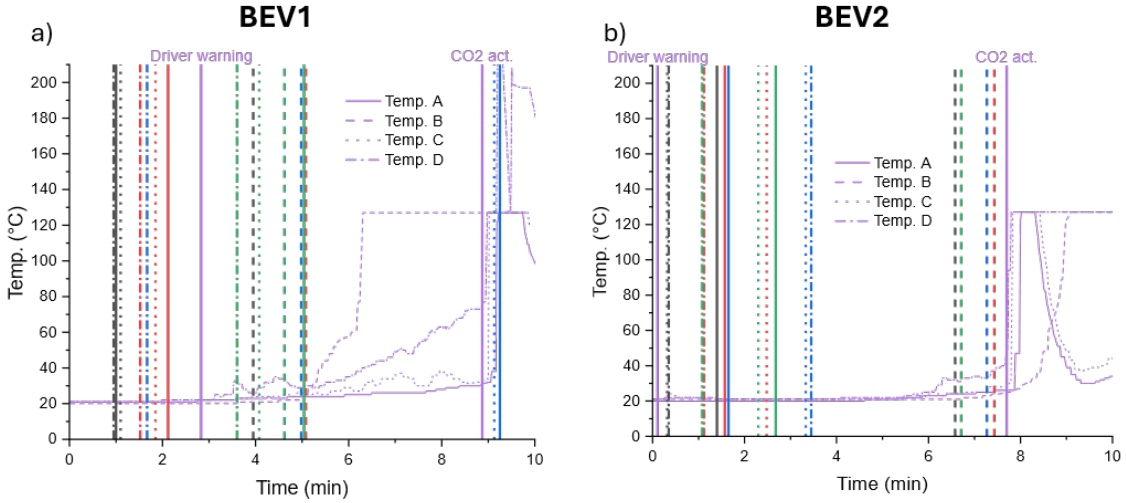

Figure 3. Alarm activation times (vertical lines) for the different sensors (BLACK – Li-ion Tamer, RED – EC CO, BLUE – EC H_2, and GREEN – Ind. fire det.) for a) BEV1 and b) BEV2. Sensors' position is indicated by line style; A – solid, B – dash, C – dot, and D – dash dot. Temperature readings from the industrial fire detector are presented in background. Vertical purple lines indicate time of warning message at the driver display and activation of the carbon dioxide suppression system.

© RISE Research Institutes of Sweden

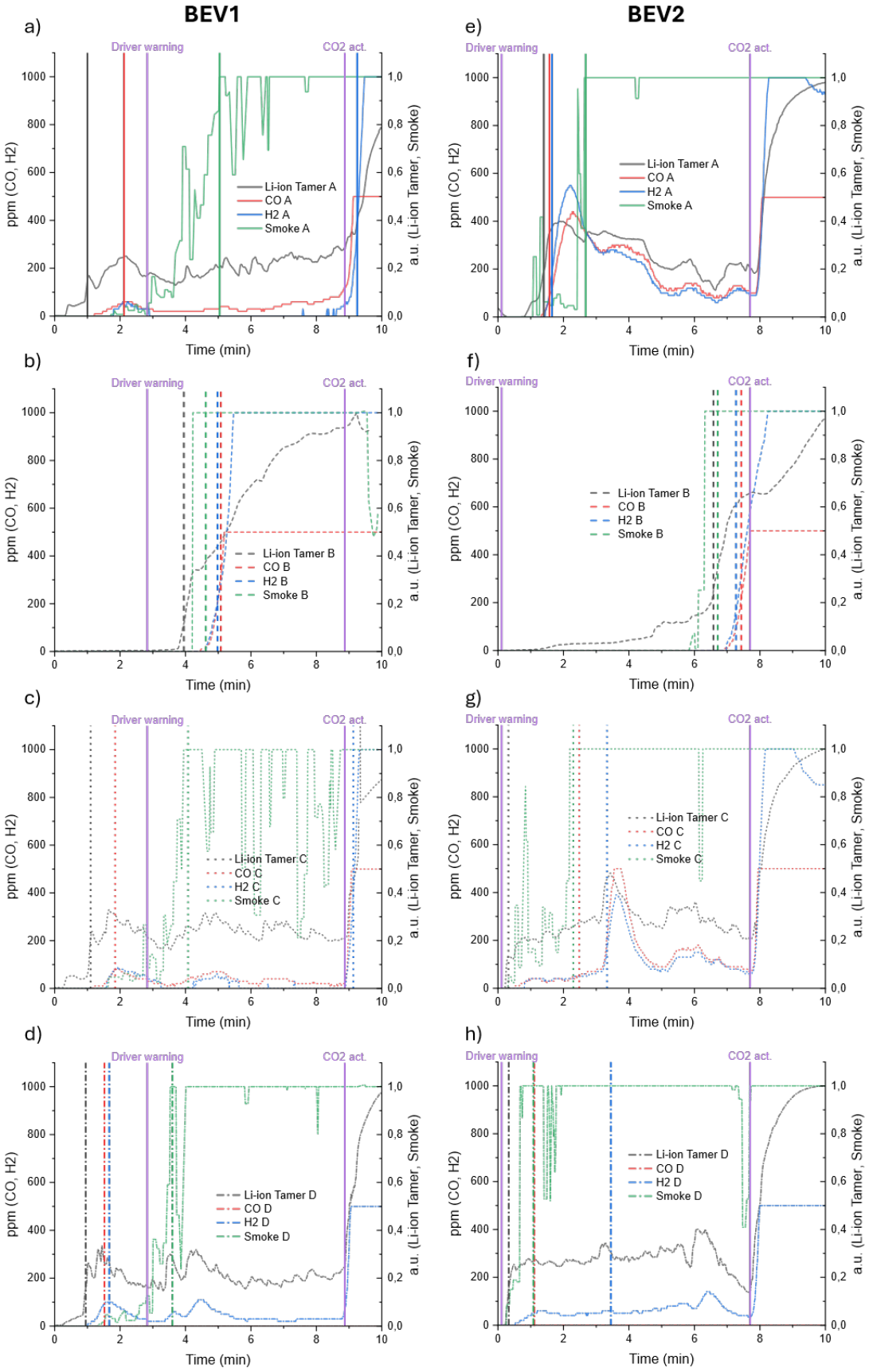

Figure 4. Sensors' alarm activation times together with raw signal (ppm levels for EC CO and EC H_2 and normalized values for Li-ion Tamer and Ind. fire det.) for BEV1 (a-d) and BEV2 (e-h) in the four different sensor positions (A-D).

© RISE Research Institutes of Sweden

Overall, looking at both tests, fastest response was attained in the ceiling position, while second fastest response differed between wall and floor positions. The Li-ion Tamer sensor was fastest followed by the EC CO sensor. The fire detector had similar response time as the EC CO sensor in the BEV2 test but was clearly slower in the BEV1 test. The EC H_2 sensor had also similar response time as the EC CO sensor in some positions in both tests but were clearly slower in other positions. As seen in Figure 4, the concentrations of CO and H_2 are very similar, why the differences in response times are probably due to the differences in alarm thresholds (50 ppm for EC CO and 100 ppm for EC H_2). Note that the CO concentrations in Figure 4d and 4h (ceiling position) are missing due to logging problems.

The maximum differences in alarm time for a given sensor type across the three positions outside the vehicle cabin were 65 s for Li-ion Tamer, 80 s for EC CO, 110 s for EC H_2 (BEV2 test), and 95 s for the industrial fire detector. The maximum differences in alarm time between the sensor types at each position (excluding the EC H_2 sensors that alarmed after the CO_2 activation) were 245 s at position A (on the floor), 60 s at position B (inside vehicle cabin), 180 s at position C (on the wall), and 185 s in D (in the ceiling). The result indicates that both sensor type and sensor position have a significant effect on the alarm response time. However, in these two tests, sensor type had a greater effect on response time than sensor position, considering positions at similar distance from the vehicle.

3.2.1 Continuous monitoring

The sensor data obtained after activation of the CO_2 suppression system provide insights into the conditions within the enclosure during the later stages of the tests. Although continuous monitoring was not a primary objective, the results are of interest from a firefighting perspective, particularly regarding the presence and concentration of flammable gases. Figure 5 shows the raw signals from the sensors positioned on the floor (A) and on the wall (C) throughout the approximately 3 hours duration of both tests. Unfortunately, the upper measurements limits of the EC CO and EC H_2 sensors (500 ppm and 1000 ppm, respectively) were exceeded, preventing quantification of higher concentrations. Therefore, other sensor types, or sensors with higher measurement ranges, are required to measure concentrations approaching the lower explosion limit (LEL), which is at the percentage level rather than the ppm level. Despite the limitations imposed by the sensor measurement ranges, the differences in response between the two tests shown in Figure 5 are noteworthy. For BEV1, gas and smoke concentrations remain above the upper measurement limit from activation of the CO_2 suppression system until ventilation of the test compartment. In contrast, for BEV2, the gas and smoke concentrations are steadily decreasing shortly after activation of the CO_2 suppression system. The fluctuation observed in the gas and smoke concentrations reflect the repeated discharge of supplemental CO_2 cylinders, which were activated to maintain the design oxygen concentrations within the test compartment. The need for repeated CO_2 discharge indicates dilution of gas and/or leakage of gas and smoke from the test compartment, which explains the decreasing concentration seen in Figure 5b. The same number of CO_2 discharges were required during the BEV1 test but no corresponding decrease in gas and smoke concentrations can be observed in Figure 5a. Two possible explanations are proposed. First, gas and smoke may have continued to be generated during this period for BEV1, for example

© RISE Research Institutes of Sweden

due to ongoing thermal propagation within the battery pack. Secondly, the initial gas and smoke concentrations following activation of the CO_2 suppression system may have been substantially higher in BEV1 test compared to the BEV2 test. In that case, the gas and smoke concentrations could have been decreasing over time without being visible in the data, as they remained above the upper measurement limits of the sensors throughout the period. A combination of these explanations is also possible.

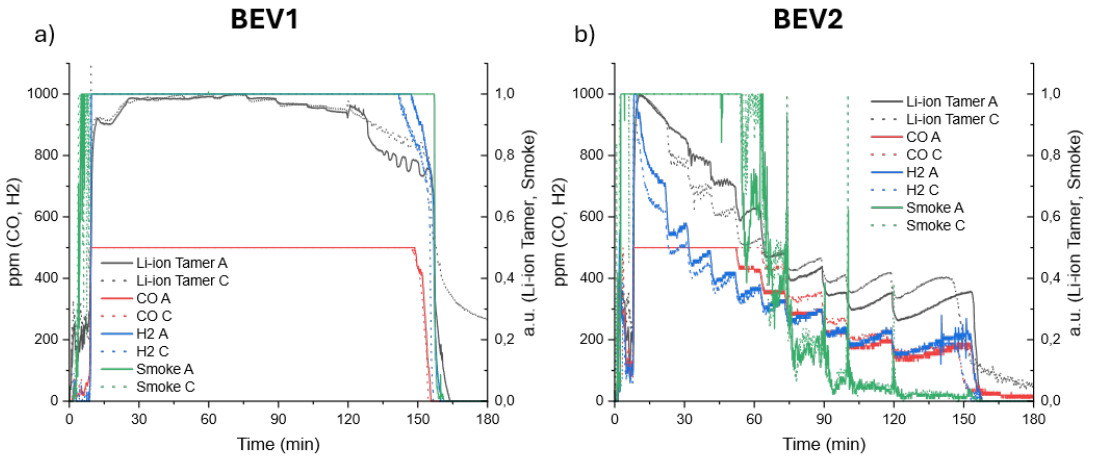

Figure 5. Sensors' raw signal (ppm levels for EC CO and EC H_2 and normalized values for Li-ion Tamer and Ind. fire det.) in position A and C for the complete test duration of approximately 3 hours for a) BEV1 and b) BEV2.

4 Conclusions

The large-scale tests demonstrated, in the scenarios investigated, that all evaluated sensor technologies could detect BEV fire events at an early stage when positioned near the vehicle. The results show that both sensor type and sensor location influence response time; however, within the tested configuration, the choice of sensor technology had a greater impact than placement around the vehicle. Among the evaluated sensors, the Li-ion Tamer consistently provided the earliest alarms and showed the highest sensitivity to the initial battery off-gassing and fire development phase. The electrochemical CO sensor was generally the second fastest detector and showed consistent performance in both tests, while the industrial fire detector and the electrochemical H_2 sensor responded well in some locations or in one of the tests but responded later in other configurations.

Sensor placement in the ceiling resulted in the fastest detection in both tests, indicating that gases and smoke generated during battery failure rapidly migrate upwards under the conditions tested. Sensors mounted on the wall and close to the floor also provided early warning, although with somewhat longer response times. Sensors located inside the vehicle cabin alarmed significantly later than sensors positioned outside the vehicle, demonstrating that hazardous gases and smoke may accumulate in the surrounding space before entering the passenger compartment, if windows and doors remain closed.

The experiments also highlighted differences in the development of the two BEV fire scenarios. The BEV2 scenario exhibited a more rapid initial development and generated vehicle warning messages at a very early stage, only seconds after fire initiation, whereas BEV1 generated a warning message after 3 min, only 1 min before

© RISE Research Institutes of Sweden

substantial amount of gas and smoke entered the vehicle cabin. Prior to activation of the CO_2 suppression system, higher concentrations of unburnt flammable gases were measured in the BEV2 scenario compared to BEV1, but after activation the concentrations of flammable gases were lower in the BEV2 scenario. Continuous monitoring after CO_2 discharge indicated that valuable information can still be obtained from gas and smoke sensors during suppression operations. However, the tested electrochemical gas sensors reached their upper measurement limits and were therefore unable to quantify potentially hazardous concentrations approaching the lower explosive limit.

Overall, the results support the use of dedicated battery off-gas detection in combination with conventional gas and fire detection technologies as part of a layered detection strategy. Further work should investigate gas sensors with extended measurement ranges to enable assessment of post-suppression conditions and improve risk assessment.

© RISE Research Institutes of Sweden

Through our international collaboration programmes with academia, industry, and the public sector, we ensure the competitiveness of the Swedish business community on an international level and contribute to a sustainable society. Our 2,800 employees support and promote all manner of innovative processes, and our roughly 100 testbeds and demonstration facilities are instrumental in developing the future-proofing of products, technologies, and services. RISE Research Institutes of Sweden is fully owned by the Swedish state.

I internationell samverkan med akademi, näringsliv och offentlig sektor bidrar vi till ett konkurrenskraftigt näringsliv och ett hållbart samhälle. RISE 2 800 medarbetare driver och stöder alla typer av innovationsprocesser. Vi erbjuder ett 100-tal test- och demonstrationsmiljöer för framtidssäkra produkter, tekniker och tjänster. RISE Research Institutes of Sweden ägs av svenska staten.

RISE Research Institutes of Sweden AB
Box 857, 501 15 BORÅS, SWEDEN
Telephone: +46 10-516 50 00
E-mail: info@ri.se, Internet: www.ri.se

RISE Report 2026:114
ISBN: 978-91-90193-49-5

© RISE Research Institutes of Sweden